



CMS-TAU-20-001

 CERN-EP-2021-257  
2022/07/18

# Identification of hadronic tau lepton decays using a deep neural network

The CMS Collaboration<sup>\*</sup>

## Abstract

A new algorithm is presented to discriminate reconstructed hadronic decays of tau leptons ( $\tau_h$ ) that originate from genuine tau leptons in the CMS detector against  $\tau_h$  candidates that originate from quark or gluon jets, electrons, or muons. The algorithm inputs information from all reconstructed particles in the vicinity of a  $\tau_h$  candidate and employs a deep neural network with convolutional layers to efficiently process the inputs. This algorithm leads to a significantly improved performance compared with the previously used one. For example, the efficiency for a genuine  $\tau_h$  to pass the discriminator against jets increases by 10–30% for a given efficiency for quark and gluon jets. Furthermore, a more efficient  $\tau_h$  reconstruction is introduced that incorporates additional hadronic decay modes. The superior performance of the new algorithm to discriminate against jets, electrons, and muons and the improved  $\tau_h$  reconstruction method are validated with LHC proton-proton collision data at  $\sqrt{s} = 13$  TeV.

*Published in the Journal of Instrumentation as doi:10.1088/1748-0221/17/07/P07023.*



## 1 Introduction

Tau leptons play a crucial role in determining the nature of the 125 GeV Higgs boson [1–5], in searching for additional Higgs bosons [6–13], and in searching for other new particles [14–16]. Since tau leptons most frequently decay to hadrons and neutrinos, all these analyses require the efficient reconstruction and identification of hadronic tau lepton decays ( $\tau_h$ ). In this paper, we introduce a new algorithm to identify  $\tau_h$  candidates coming from hadronic tau lepton decays in the CMS detector and measure its performance with collision data from the CERN LHC. The new algorithm is based on a deep neural network (DNN) that significantly improves the performance of the  $\tau_h$  identification. Furthermore, we discuss an optimized  $\tau_h$  reconstruction algorithm that includes additional  $\tau_h$  decay modes.

Hadronic tau lepton decays are reconstructed and identified as follows. First,  $\tau_h$  candidates are reconstructed in one of their decay modes with the “hadrons-plus-strips” algorithm [17–19], which reconstructs its decay mode and the visible four-momentum, i.e. the four-momentum of all decay products except for the neutrinos. Second, the  $\tau_h$  candidates are identified as coming from genuine  $\tau_h$  decays rather than from jets, electrons, and muons. Quark and gluon jets often constitute the most important source of background since they are produced abundantly in proton-proton (pp) collisions at the LHC.

Previously,  $\tau_h$  candidates were reconstructed only in their main decay modes: one-prong decays with and without  $\pi^0$ s, and three-prong decays without  $\pi^0$ s. Now, we also consider three-prong  $\tau_h$  decays with  $\pi^0$ s, which account for 7.4% of all  $\tau_h$  decays. Furthermore, three-prong  $\tau_h$  decays are recovered in which one of the charged hadrons is either not reconstructed as a charged hadron or not even as a track.

The identification of  $\tau_h$  candidates in CMS previously proceeded with separate discriminators against jets, electrons, and muons [18, 19]. The discriminators against jets and electrons combined information from high-level input variables (i.e. derived quantities, such as the transverse momentum  $p_T$  sum of particles near the  $\tau_h$  axis) using a multivariate analysis (MVA) classifier based on an ensemble of boosted decision trees. A similar approach is used for  $\tau_h$  identification by the ATLAS Collaboration [20, 21]. Our previous discriminator against muons was based on explicit thresholds of a few discriminating observables. Here, we introduce a new  $\tau_h$  identification algorithm, DEEPTAU, based on a DNN that simultaneously discriminates against jets, electrons, and muons. The DNN uses a combination of high-level inputs, similar to previous algorithms, and information from all reconstructed particles in the vicinity of the  $\tau_h$  candidate. The information from all reconstructed particles near the  $\tau_h$  axis is processed with convolutional layers [22–24] in pseudorapidity-azimuth ( $\eta$ - $\phi$ ) space. Convolutional layers have been developed in the context of image recognition and are based on the premise that a fragment of the input, e.g. an image, can be processed independently of its position, exploiting the translational invariance of the problem. In a given physics analysis, the superior performance of such an algorithm leads to an increase of the signal efficiency for a given target background rate from jets, electrons, or muons misidentified as  $\tau_h$ , which typically translates directly into superior sensitivity or precision of the analysis.

Similar approaches have been proposed and employed in the context of  $\tau_h$  reconstruction and identification as well as in the classification of jets. Identification algorithms for  $\tau_h$  using shallow neural networks were studied at LEP [25]. The ATLAS Collaboration developed an algorithm to identify visible  $\tau_h$  decay products with a recurrent DNN [26]. The ATLAS and CMS Collaborations also use DNNs to identify jets as coming from decays of b quarks [27–30]. In particular, the DEEPJET algorithm [30] employs multiclass classification to identify jets as coming from gluons, leptons, b quarks, c quarks, or light quarks. Convolutional layers have

---

been used in algorithms that identify large-radius jets as originating from the decays of high- $p_T$  heavy particles, e.g. in the DEEPAK8 algorithm that identifies jets with  $p_T > 200 \text{ GeV}$  as coming from decays of top quarks or decays of W, Z, or Higgs bosons [31].

This paper is structured as follows. After an overview of the CMS detector and the event reconstruction in Section 2, the recent advances in the  $\tau_h$  reconstruction are discussed in Section 3. Section 4 describes the new  $\tau_h$  identification algorithm based on neural networks and gives an overview of its performance with simulated events. The performance of the algorithm with LHC collision events is then discussed in Section 5. The paper is summarized in Section 6. Tabulated results are provided in the HEPData record for this analysis [32].

## 2 The CMS detector

The central feature of the CMS apparatus is a superconducting solenoid of 6 m internal diameter, providing a magnetic field of 3.8 T. Within the solenoid volume are a silicon pixel and strip tracker, a lead tungstate crystal electromagnetic calorimeter (ECAL), and a brass and scintillator hadron calorimeter (HCAL), each composed of a barrel and two endcap sections. Forward calorimeters extend the  $\eta$  coverage provided by the barrel and endcap detectors. Muons are detected in gas-ionization chambers embedded in the steel flux-return yoke outside the solenoid. A more detailed description of the CMS detector, together with a definition of the coordinate system used and the relevant kinematic variables, is reported in Ref. [33].

### 2.1 Event reconstruction

The particle-flow (PF) algorithm [34] reconstructs and identifies each individual particle in an event, with an optimized combination of information from the various elements of the CMS detector. The energy of photons is obtained from the ECAL measurement. The energy of electrons is determined from a combination of the electron momentum at the primary interaction vertex, as determined by the tracker, the energy of the corresponding ECAL cluster, and the energy sum of all bremsstrahlung photons spatially compatible with originating from the electron track. The energy of muons is obtained from the curvature of the corresponding track. The energy of charged hadrons is determined from a combination of their momentum measured in the tracker and the matching ECAL and HCAL energy deposits, corrected for the response function of the calorimeters to hadronic showers. Finally, the energy of neutral hadrons is obtained from the corresponding corrected ECAL and HCAL energies.

For each event, hadronic jets are clustered from all the PF candidates using the infrared- and collinear-safe anti- $k_T$  algorithm [35, 36] with a distance parameter of 0.4. Jet momentum is determined as the vectorial sum of all particle momenta in the jet, and the simulation is, on average, within 5 to 10% of the true momentum over the whole  $p_T$  spectrum and detector acceptance. Additional pp interactions within the same or nearby bunch crossings (pileup) can contribute additional tracks and calorimetric energy depositions, increasing the apparent jet momentum. To mitigate this effect, charged particles identified as originating from pileup vertices are discarded and an offset correction is applied to correct for remaining contributions [37]. Jet energy corrections are derived from simulation to bring the measured response of jets to that of particle-level jets on average. In situ measurements of the momentum balance in dijet, photon+jet, Z+jet, and multijet events are used to correct any residual differences in the jet energy scale between data and simulation [38]. Additional selection criteria are applied to each jet to remove jets potentially dominated by instrumental effects or reconstruction failures [37].

The missing transverse momentum vector  $\vec{p}_T^{\text{miss}}$  is computed as the negative vector sum of

the transverse momenta of all the PF candidates in an event, and its magnitude is denoted as  $p_T^{\text{miss}}$  [39]. The  $\vec{p}_T^{\text{miss}}$  is modified to include corrections to the energy scale of the reconstructed jets in the event.

The candidate vertex with the largest value of summed physics-object  $p_T^2$  is the primary pp interaction vertex. The physics objects specifically used for this purpose are jets, clustered using the jet finding algorithm [35, 36] with the tracks assigned to candidate vertices as inputs, and the associated missing transverse momentum, taken as the negative vector sum of the  $p_T$  of those jets, which include tracks from leptons.

Muons are measured in the range  $|\eta| < 2.4$ , with detection planes made using three technologies: drift tubes, cathode strip chambers, and resistive plate chambers. The single muon trigger efficiency exceeds 90% over the full  $\eta$  range, and the efficiency to reconstruct and identify muons is greater than 96%. Matching muons to tracks measured in the silicon tracker results in a relative  $p_T$  resolution for muons with  $p_T < 100 \text{ GeV}$  of 1% in the barrel and 3% in the endcaps. The  $p_T$  resolution in the barrel is better than 7% for muons with  $p_T < 1 \text{ TeV}$  [40].

The electron momentum is estimated by combining the energy measurement in the ECAL with the momentum measurement in the tracker. The momentum resolution for electrons with  $p_T \approx 45 \text{ GeV}$  from  $Z \rightarrow ee$  decays ranges from 1.7 to 4.5%. It is generally better in the barrel region than in the endcaps, and also depends on the bremsstrahlung energy emitted by the electron as it traverses the material in front of the ECAL [41].

Events of interest are selected using a two-tiered trigger system. The first level, composed of custom hardware processors, uses information from the calorimeters and muon detectors to select events at a rate of around 100 kHz within a fixed latency of about  $4 \mu\text{s}$  [42]. The second level, known as the high-level trigger, consists of a farm of processors running a version of the full event reconstruction software optimized for fast processing, and reduces the event rate to around 1 kHz before data storage [43].

## 2.2 Simulated event samples

Monte Carlo simulated event samples are used to optimize the  $\tau_h$  reconstruction, as input for the training of the neural network, and to validate the performance of the  $\tau_h$  reconstruction and identification. Unless explicitly mentioned, the simulated event samples include decays to all leptons ( $\ell$ ), i.e. to electrons, muons, and tau leptons. The samples listed in the following are produced separately for conditions corresponding to the 2016, 2017, and 2018 data-taking periods; a range of versions of the different generators is used as specified below.

Events from the production of  $Z/\gamma^*$  and W bosons in association with jets (Z+jets and W+jets) are generated with MADGRAPH5\_aMC@NLO v2.2.2 or v2.4.2 [44] at leading order (LO) in perturbative quantum chromodynamics (QCD) with the MLM jet merging scheme [45]. A separate Z+jets sample for the training, as well as diboson event samples (WW, WZ, and ZZ), are generated with MADGRAPH5\_aMC@NLO at next-to-leading order (NLO) in perturbative QCD with the FxFx merging scheme [46]. Events from top quark-antiquark pair ( $t\bar{t}$ ) and single top quark production are generated with POWHEG v2.0 at NLO in perturbative QCD [47–52]. Events from multijet production via the strong interaction, referred to as QCD multijet production, are generated at LO using PYTHIA 8.223, 8.226, or 8.230 [53]. The PYTHIA event generator is also used to produce heavy additional gauge boson event samples at LO,  $Z' \rightarrow \ell\ell$ , with  $m(Z')$  ranging from 1 to 5 TeV. The generation of 125 GeV Higgs boson (H) events via gluon fusion at NLO with H decays to tau leptons ( $H \rightarrow \tau\tau$ ) is also performed with the POWHEG 2.0 generator [54]. The NNPDF 3.0 or 3.1 parton distribution functions are used as input in all the calculations [55, 56].

The PYTHIA program is used to simulate tau lepton decays, parton showering, hadronization, and multiparton interactions, with version 8.223, 8.226, or 8.230 and tune CUETP8M1 or CP5 [57]. For the  $Z' \rightarrow \ell\ell$  samples, TAUOLA is used instead to simulate tau lepton decays [58]. Pileup interactions are generated with PYTHIA and are overlaid on all simulated events according to the luminosity profile of the considered data. All generated events are passed through a detailed simulation of the CMS detector with GEANT4 [59]. The simulated and recorded events are reconstructed with the same CMS reconstruction software.

### 3 The $\tau_h$ reconstruction

The reconstruction of  $\tau_h$  candidates is carried out with the hadrons-plus-strips algorithm. The reconstruction proceeds in four steps, as summarized in the following and described in detail in Refs. [17–19].

First, seed regions are defined, with the goal of reconstructing one  $\tau_h$  candidate per seed region. Each seed region is defined by a reconstructed hadronic jet. The jets for the seeding are clustered from all particles reconstructed by the PF algorithm using the anti- $k_T$  algorithm with a distance parameter of  $R = 0.4$ . All particles in an  $\eta$ - $\phi$  cone of radius  $\Delta R \equiv \sqrt{\Delta\eta^2 + \Delta\phi^2} = 0.5$  around the jet axis are considered for the next steps of the  $\tau_h$  reconstruction.

Second,  $\pi^0$  candidates are reconstructed using “strips” in  $\eta$ - $\phi$  space in which the four-momenta of electrons and photons are added, and charged-hadron ( $h^\pm$ ) candidates are selected using charged particles from the PF algorithm as input.

Third, all possible  $\tau_h$  candidates are reconstructed in a number of decay modes from the reconstructed charged hadrons and strips. The  $\tau_h$  four-momentum is obtained from summing the four-momenta of the charged hadrons and strips used to reconstruct the  $\tau_h$  candidate in a given decay mode. An overview of the  $\tau$  decay modes and their branching fractions is given in Table 1. There are seven different reconstructed  $\tau_h$  decay modes, including three new ones (with respect to the algorithm documented in Ref. [19]) that target  $\tau^- \rightarrow h^- h^+ h^- \pi^0 \nu_\tau$  decays and  $\tau_h$  decays with three charged hadrons of which one is not reconstructed as a charged particle:

1.  $h^\pm$ , targeting  $\tau^- \rightarrow h^- \nu_\tau$  decays (charge-conjugate decays are implied);
2.  $h^\pm \pi^0$ , targeting  $\tau^- \rightarrow h^- \pi^0 \nu_\tau$  decays;
3.  $h^\pm \pi^0 \pi^0$ , targeting  $\tau^- \rightarrow h^- \pi^0 \pi^0 \nu_\tau$  decays;
4.  $h^\pm h^\mp h^\pm$ , targeting  $\tau^- \rightarrow h^- h^+ h^- \nu_\tau$  decays;
5.  $h^\pm h^\mp h^\pm \pi^0$  (new), targeting  $\tau^- \rightarrow h^- h^+ h^- \pi^0 \nu_\tau$  decays;
6.  $h^\pm h^{\pm/\mp}$  (new), targeting  $\tau^- \rightarrow h^- h^+ h^- \nu_\tau$  decays;
7.  $h^\pm h^{\pm/\mp} \pi^0$  (new), targeting  $\tau^- \rightarrow h^- h^+ h^- \pi^0 \nu_\tau$  decays.

Fourth, a single  $\tau_h$  candidate is chosen among all possible reconstructed  $\tau_h$  candidates within a seed region. Reconstructed  $\tau_h$  candidates are subject to the following constraints:

Table 1: [

Tau lepton decays and their branching fractions.] Decays of  $\tau$  leptons and their branching fractions ( $\mathcal{B}$ ) in % [60]. The known intermediate resonances of all the listed hadrons are indicated where appropriate. Charged hadrons are denoted by the symbol  $h^\pm$ . Although only  $\tau^-$  decays are shown, the decays and values of the branching fractions are identical for

Decay mode	Resonance	$\mathcal{B}$ (%)
Leptonic decays		35.2
$\tau^- \rightarrow e^- \bar{\nu}_e \nu_\tau$		17.8
$\tau^- \rightarrow \mu^- \bar{\nu}_\mu \nu_\tau$		17.4
Hadronic decays		64.8
charge-conjugate decays.		
$\tau^- \rightarrow h^- \nu_\tau$		11.5
$\tau^- \rightarrow h^- \pi^0 \nu_\tau$	$\rho(770)$	25.9
$\tau^- \rightarrow h^- \pi^0 \pi^0 \nu_\tau$	$a_1(1260)$	9.5
$\tau^- \rightarrow h^- h^+ h^- \nu_\tau$	$a_1(1260)$	9.8
$\tau^- \rightarrow h^- h^+ h^- \pi^0 \nu_\tau$		4.8
Other		3.3

- The mass of the reconstructed  $\tau_h$  candidate is required to be loosely compatible with: (i) the  $\rho(770)$  resonance if reconstructed in the  $h^\pm \pi^0$  mode; (ii) the  $a_1(1260)$  resonance if reconstructed in either of the  $h^\pm \pi^0 \pi^0$  and  $h^\pm h^\mp h^\pm$  modes [19]; or (iii) the expected mass spectrum including the  $\rho(1450)$  resonance if reconstructed in the  $h^\pm h^\mp h^\pm \pi^0$  modes. The mass of all  $h^\pm$  candidates is assumed to be the charged-pion mass, in line with the output from the PF algorithm.
- The  $\tau_h$  charge needs to correspond to  $\pm 1$ , unless the  $\tau_h$  candidate is reconstructed in a mode with a missed charged hadron, in which case the charge is set to correspond to the charge of the charged hadron with higher  $p_T$ .
- All reconstructed  $h^\pm$  and  $\pi^0$  need to be in the signal cone, defined with radius  $\Delta R = 3.0/p_T(\text{GeV})$  (with  $\Delta R$  limited to the range 0.05–0.1) with respect to the  $\tau_h$  momentum.

Among the selected  $\tau_h$  candidates, the one with the highest  $p_T$  is chosen. This  $\tau_h$  candidate can subsequently be discriminated against quark or gluon jets, electrons, and muons.

A large fraction of  $\tau_h$  decays are reconstructed in their targeted decay modes, as inferred from Fig. 1, which shows the fractions of reconstructed decay modes for generated  $\tau_h$  with a given decay mode that fulfil  $p_T > 20 \text{ GeV}$  and  $|\eta| < 2.3$ . The fraction of generated  $\tau_h$  not reconstructed in any of the modes ranges from 11% for  $h^\pm$  to 25% for  $h^\pm \pi^0$ . The overall reconstruction efficiency is mostly limited by the ability to reconstruct tracks from charged hadrons of around 90% [34]. For the decay modes without missing charged hadrons, the charge assignment is 99% correct for an average  $Z \rightarrow \tau\tau$  event sample, 98% for  $\tau_h$  with  $p_T \approx 200 \text{ GeV}$ , and 92% for  $\tau_h$  with  $p_T \approx 1 \text{ TeV}$ .

The decay modes with missing charged hadrons recover 19% of the  $\tau^- \rightarrow h^- h^+ h^- \nu_\tau$  decays and 13% of the  $\tau^- \rightarrow h^- h^+ h^- \pi^0 \nu_\tau$  decays. However, because of the missing charged hadron, the charge assignment is only correct in  $\approx 70\%$  of the cases, as opposed to an average of 99% for the other decay modes. Since most physics analyses apply requirements on the reconstructed  $\tau_h$  charge to suppress background events, these decay modes are only useful for analyses that are not limited by background events. None of the current analyses within the CMS Collaboration fall into this category. Although we include the decay modes with missing charged hadrons in the new  $\tau_h$  identification algorithm, most of the subsequent results are shown only

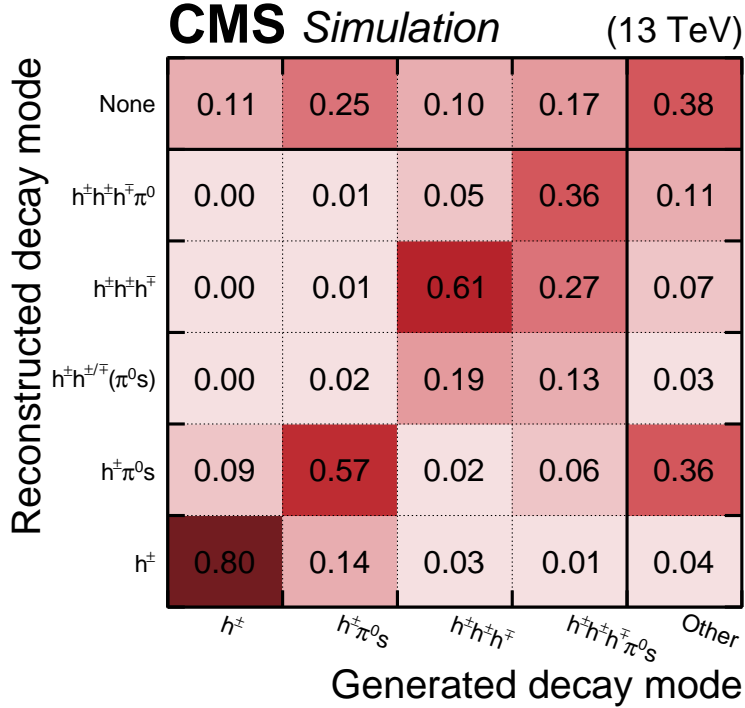


Figure 1: Decay mode confusion matrix. For a given generated decay mode, the fractions of reconstructed  $\tau_h$  in different decay modes are given, as well as the fraction of generated  $\tau_h$  that are not reconstructed. Both the generated and reconstructed  $\tau_h$  need to fulfil  $p_T > 20\text{ GeV}$  and  $|\eta| < 2.3$ . The  $\tau_h$  candidates come from a  $Z \rightarrow \tau\tau$  event sample with  $m_{\tau\tau} > 50\text{ GeV}$ . Decay modes with the same numbers of charged hadrons and one or two  $\pi^0$ s are combined and labelled as “ $\pi^0$ s”.

for reconstructed  $\tau_h$  candidates in one of the other decay modes, unless explicitly stated.

## 4 The $\tau_h$ identification with a deep neural network

The newly developed  $\tau_h$  identification algorithm uses a deep neural network structure. Its architecture is based on the following three premises:

- Multiclass: Previously, separate dedicated algorithms were used to reject electrons, muons, or quark and gluon jets reconstructed as a  $\tau_h$  candidate, either based on tree ensembles (jets and electrons) or on a number of selection criteria (muons) [19]. Including electrons, muons, and jets in the same algorithm is expected to both improve identification performance and to reduce maintenance efforts.
- Usage of lower-level information: The MVA discriminators used previously were built on higher-level input variables and showed improved performance with respect to cutoff-based criteria. However, jets hadronize and fragment in complex patterns, and particles from concurrent interactions lead to similarly complex detector patterns. We expect that a machine-learned algorithm, which uses a sufficiently large data set for the training and is able to exploit lower-level information, can lead to improved performance. Therefore, information about all reconstructed particles near the  $\tau_h$  candidate is directly used as input to the algorithm.
- Domain knowledge: Sets of handcrafted higher-level input variables used previ-

ously are utilized as additional inputs to the information about the single reconstructed particles. Although it should, in principle, be possible to achieve the same performance with and without using these variables given a sufficiently large set of events for the training and a suitable network architecture, the usage of the higher-level inputs may reduce the number of training events needed and improve the convergence of the training, as seen in other studies [30].

Various network architectures were considered under the constraints that they satisfy these premises with manageable complexity. In particular, the algorithm must be trainable on the available hardware, and both its memory footprint and evaluation time are subject to constraints when used in the CMS reconstruction. To process the information on all reconstructed particles near the  $\tau_h$  axis, convolutional layers are employed. Compared with other approaches like fully connected layers or graph-based structures, convolutional layers have two main advantages: they have a smaller computational complexity and they are implemented efficiently in current deep learning software. On the other hand, they require a partitioning of inputs, in the case at hand a two-dimensional one in  $\eta$ - $\phi$  space. As explained in the following, this partitioning both leads to many empty input cells and cells in which information is lost since multiple particles are found. The details of the architecture and the inputs are given in the following.

## 4.1 Inputs

### 4.1.1 Particle-level inputs

Two grids are defined in  $\eta$ - $\phi$  space, centred around the  $\tau_h$  axis, as displayed in Fig. 2: an inner grid with  $11 \times 11$  cells and a grid size of  $0.02 \times 0.02$ , and an outer grid with  $21 \times 21$  cells and grid size of  $0.05 \times 0.05$ . These two grids overlap, i.e. the information in the inner grid will also be part of the information that is processed by the outer grid. For each grid cell, properties of contained reconstructed particles of seven different types are used as inputs. If there is more than one particle of a given type, only the highest  $p_T$  particle is used as input. The various types are the five kinds of particles reconstructed by the PF algorithm in the central detector, i.e. muons, electrons, photons, charged hadrons, and neutral hadrons. The muons and electrons are reconstructed by dedicated standalone reconstruction algorithms, which provide more specific information to distinguish them from the other particles. For each particle, various types of information are taken into account, as listed in Table 2. The major tradeoffs defining the grid size are the computational cost and the loss of information when more than one particle of a specific type is present in a grid cell. On average, 1.7% of the inner and 7.1% of the outer grid cells are occupied. Up to approximately 10% of the occupied cells contain more than one particle of a specific type.

The finer binning near the  $\tau_h$  axis is motivated as follows: First, the  $\tau_h$  decay products occur predominantly in an  $\eta$ - $\phi$  cone with radius 0.1 around the reconstructed  $\tau_h$  axis. Second, high- $p_T$  jets are more collimated, so a finer grid is needed to capture all particles within them.

### 4.1.2 High-level inputs

The high-level input variables correspond primarily to those proven to be useful in the previous MVA classifier [19]. These variables include: (i) the  $\tau_h$  four-momentum and charge; (ii) the number of charged and neutral particles used to reconstruct the  $\tau_h$  candidate; (iii) isolation variables; (iv) the compatibility of the leading  $\tau_h$  track with coming from the PV; (v) the properties of a secondary vertex in case of a multiprong  $\tau_h$ ; (vi) observables related to the  $\eta$  and  $\phi$  distributions of energy reconstructed in the strips; (vii) observables related to the compatibility

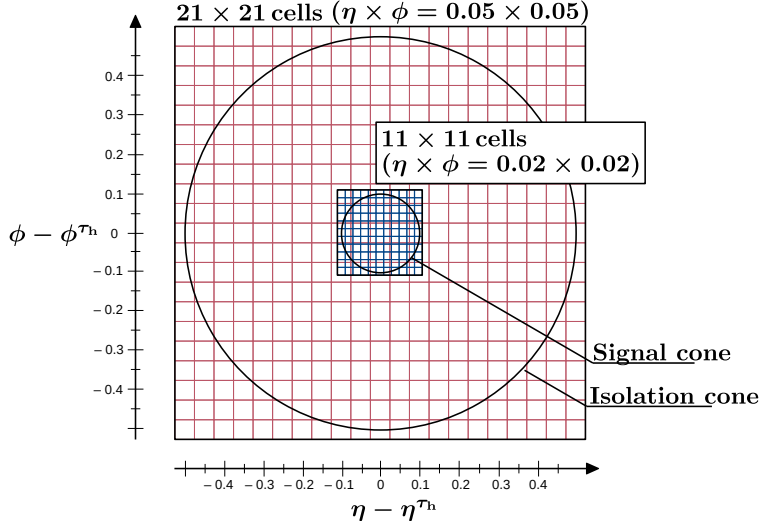


Figure 2: Layout of the grids in  $\eta$ - $\phi$  space around the reconstructed  $\tau_h$  axis used to process the particle-level inputs for the convolutional layers of the DNN. The inner grid comprises  $11 \times 11$  cells with a grid size of  $0.02 \times 0.02$  and contains the signal cone with a radius of  $0.05\text{--}0.1$ , which is defined in the  $\tau_h$  reconstruction (the charged hadrons and  $\pi^0$  candidates used to reconstruct the  $\tau_h$  candidate need to be within the signal cone). For high- $p_T$  quark and gluon jets, the finer grid is also able to resolve the dense core of the jet. The outer grid comprises  $21 \times 21$  cells with a grid size of  $0.05 \times 0.05$  and contains the isolation cone with a radius of  $0.5$  that is used to define higher-level observables that correlate with quark or gluon jet activity.

Table 2: [

Per-particle input variables.] Input variables used for the various kinds of particles that are contained in a given cell. For each type of particle, basic kinematic quantities ( $p_T, \eta, \phi$ ) are included but not listed below. Similarly, the reconstructed charge is included for all charged particles. An estimated per-particle probability for the particle to come from a pileup interaction using the pileup identification (PUPPI) algorithm [61] is labelled as PUPPI. A number of input variables that give the compatibility of the track with the primary interaction vertex (PV) or a possible secondary vertex (SV) from the  $\tau_h$  reconstruction are denoted as “Track PV” and “Track SV”.

Particle	$N_{\text{var}}$	Inputs
PF charged hadron	27	Track PV/SV/quality, PUPPI, HCAL energy fraction
PF neutral hadron	7	PUPPI, HCAL energy fraction
Electron	37	Electron track quality, track/cluster matching, cluster shape
PF electron	22	Track PV/SV/quality, PUPPI
PF photon	23	Track PV/SV/quality, PUPPI
Muon	37	Track quality, muon station hits, ECAL deposits
PF muon	23	Track PV/SV/quality, PUPPI

of the  $\tau_h$  candidate with being an electron; and (viii) the estimated pileup density in the event. In all, there are 47 high-level input variables.

#### 4.1.3 Transformations

Input variables that are either integer in nature or have a significantly skewed distribution are modified with a linear transformation such that the values lie in the intervals  $[-1, 1]$  or

$[0, 1]$ . Most of the other input variables are subject to a standardization procedure,  $x \rightarrow (x - \mu)/\sigma$ , with  $\mu$  denoting the mean of the distribution of  $x$  and  $\sigma$  its standard deviation. The standardized inputs are truncated to  $[-5, 5]$  to protect against outliers.

## 4.2 Architecture

The overall DNN architecture is visualized in Fig. 3. The goal of the DNN is to use and process the inputs to optimally classify the  $\tau_h$  candidate as belonging to a target class, which corresponds to determining whether the reconstructed  $\tau_h$  originates from a genuine  $\tau_h$ , a muon, an electron, or a quark or gluon jet. Three different subnetworks are created that independently process the inputs from the high-level variables, the outer cells, and the inner cells. The outputs from these three subnetworks are then concatenated and passed through four fully connected layers with 200 nodes each and then to a final layer with four nodes that yield outputs  $x_\alpha$ , with  $\alpha \in \{\text{jet}, \mu, \text{e}\}$ . A softmax activation function [62],

$$y_\alpha = \exp(x_\alpha) / \sum_\beta \exp(x_\beta), \quad (1)$$

is then applied to yield estimates  $y_\alpha$  of the probabilities for the  $\tau_h$  candidate to come from each of the four target classes ( $\tau_h$ , jet,  $\mu$ , e).

The two subnetworks that process the inputs from the inner and outer cells have similar structures. As explained above, the main idea is to process the grids with convolutional layers [22–24]. In our case, the large number of input parameters for each cell makes it computationally too expensive to directly process the grid cells. To reduce the dimensionality, the inputs from each cell of the inner and outer grid are first sent through a number of fully connected layers. Since these layers act on single cells of the grids, with the full grid later on processed with convolutional layers, these fully connected layers can also be considered as one-dimensional convolutional layers, and the nodes can be considered as filters. For each cell, inputs from the electron, muon, and hadron blocks are first processed separately in three fully connected layers with a decreasing number of nodes. The outputs from the three separate processing blocks are then concatenated and passed through four additional fully connected layers with a decreasing number of nodes. The 188 input parameters are reduced to 64 output parameters (filters) for each cell that are input to the convolutional layers.

The convolutional layers each make use of 64 filters with size  $3 \times 3$ . These filters reduce the size of the grid with each step by two in each dimension since no padding is applied (i.e. the grid is not artificially extended with additional cells beyond the dimension of the grid). For both the inner cells with a dimension of  $11 \times 11$  and the outer cells with a dimension of  $21 \times 21$ , the convolutional layers are applied until the grid is reduced to a single cell. As a consequence, there are 5 convolutional layers for the inner cells and 10 for the outer cells. For both the inner and the outer cells, the final single cell implies that there are 64 outputs.

The 47 high-level input variables are processed by three fully connected layers with 113, 80, and 57 nodes, yielding 57 outputs. Taken together, the three subnetworks yield 185 output parameters that are processed through a number of fully connected layers as explained above.

After each of the fully connected and convolutional layers, batch normalization [63] and dropout regularization [64, 65] with a dropout rate of 0.2 are applied. Furthermore, nonlinearity is introduced by applying the parametric rectified linear unit activation function, which is given by  $\alpha x$  for  $x < 0$  and by  $x$  for  $x \geq 0$ , with  $\alpha$  being a trainable parameter [66].

A few alternative approaches were tried. First, networks using only high-level inputs and an overall lower number of trainable parameters were tested. These showed significantly inferior

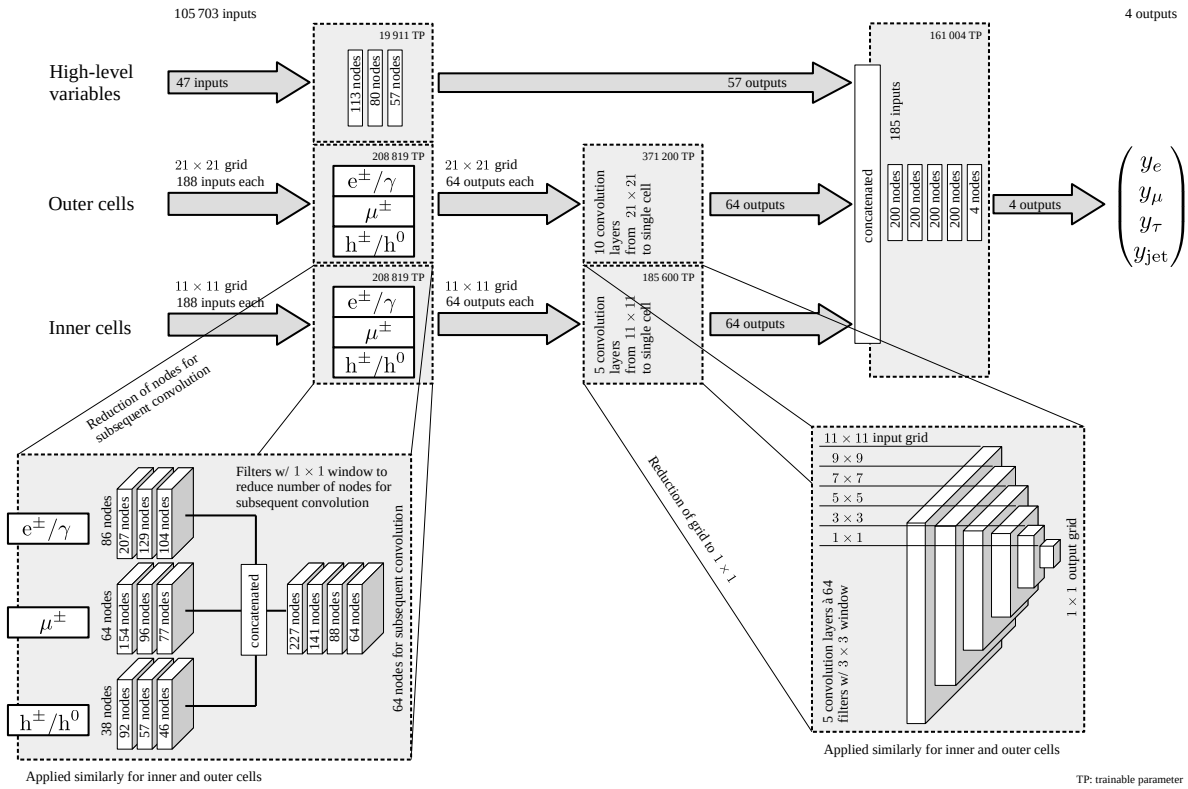


Figure 3: The DNN architecture. The three sets of input variables (inner cells, outer cells, and high-level features) are first processed separately through different subnetworks, whose outputs are then concatenated and processed through five fully connected layers before the output is calculated that gives the probabilities for a candidate to be either a  $\tau_h$ , an electron, a muon, or a quark or gluon jet. The subnetwork for the high-level inputs consists of three fully connected layers with decreasing numbers of nodes, taking 47 inputs and yielding 57 outputs. The features of both the inner and outer cells are input to complex subnetworks. In the first part, the observables in each grid cell are processed through a set of fully connected layers, first separately for electrons/photons (containing both the features for PF electrons and electrons from the standalone reconstruction), muons (similarly containing both features from PF and standalone muons), and charged/neutral hadrons, passing through three fully connected layers each. The outputs are concatenated and passed through four additional fully connected layers, yielding 64 outputs for each cell. The grids are then processed with convolutional layers, which successively reduce the size of the grid. For the inner cells, there are hence 5 convolutional layers that reduce the grid from  $11 \times 11$  to a single cell; for the outer cells, there are 10 convolutional layers that reduce the grid from  $21 \times 21$  to a single cell. The numbers of trainable parameters (TP) for the different subnetworks are also given for the different subnetworks.

performance in terms of  $\tau_h$  identification efficiency versus the misidentification probabilities for jets, electrons, and muons, as clarified in Figs. 4, 6, and 7. Second, alternative approaches were tried that were based on the idea of having two-dimensional grids for the particle-level inputs, but with different input cell sizes and with differently organized convolutional layers, e.g. convolutional layers with padding and pooling (combining the information from a number of nearby cells). The chosen architecture yielded the best performance among the ones tested within the predefined computing constraints.

### 4.3 Loss function and classifier training

The loss function is a sum of three different terms, given the four target classes (jet,  $\mu$ , e,  $\tau_h$ ):

1. a regular cross-entropy term [62] for the  $\tau_h$  target class,
2. a term implementing focal loss [67] for the binary classification of  $\tau_h$  against all backgrounds combined, and
3. another focal-loss term with three components for the classification as  $\mu$ , e, or jet, each combined with a smoothed step function that is nonzero only for  $\tau_h$  candidates that are sufficiently likely to be classified as  $\tau_h$ .

The introduction of the two focal-loss terms gives superior performance compared with using cross-entropy only. It is motivated by two considerations. First, analyses with  $\tau_h$  candidates in the final state, like the ones mentioned in the introduction, show the highest sensitivity for efficiencies in the range 50–80%, whereas performance for the highest efficiencies and purities is less important. Second, the classification performance as  $\tau_h$  is more important than the classification as e,  $\mu$ , or jet; particularly in the high-purity regime where it is less important to distinguish between the three other classes. The full definition of the loss function is given in Appendix A.

For the training, events from the following simulated processes are used: Z+jets (NLO), W+jets,  $t\bar{t}$ ,  $Z' \rightarrow \tau\tau$ ,  $Z' \rightarrow ee$ ,  $Z' \rightarrow \mu\mu$  (with  $m(Z')$  ranging from 1 to 5 TeV), and QCD multijet production. For testing, additional event samples are used, including  $H \rightarrow \tau\tau$  and Z+jets (LO) event samples, and more event samples corresponding to the processes used for the training. The event samples are simulated and reconstructed according to the 2017 data-taking conditions. The prospective  $\tau_h$  candidates need to fulfil  $p_T > 20$  GeV and  $|\eta| < 2.3$ . The  $\tau_h$  candidates are sampled from the various event samples such that the contributions of the different classes (jet,  $\mu$ , e,  $\tau_h$ ) and in different  $(p_T, \eta)$  bins are the same. Additional weights are added to make the distributions from the different classes uniform within each  $(p_T, \eta)$  bin. In total, around 140 million  $\tau_h$  candidates are used for the training, whereas 10 million are assigned as the validation samples.

The loss function is minimized with Nesterov-accelerated adaptive momentum estimation [68], which combines the *Adam* algorithm [69] with Nesterov momentum. The training setup uses the KERAS library [70] with TENSORFLOW [71] as backend. The training was carried out with a single Nvidia GeForce RTX™ 2080 graphics processing unit. The training of the final classifier was run for 10 epochs, with the training for an epoch lasting 69 hours on average. The best performance on the validation samples has been obtained after 7 epochs.

The final discriminators against jets, muons, and electrons are given by

$$D_\alpha(\mathbf{y}) = \frac{y_\tau}{y_\tau + y_\alpha}, \quad (2)$$

with  $y_\alpha$  taken from Eq. (1) and  $\alpha \in \{\text{jet}, \mu, \text{e}\}$ . In the following, these discriminators are labelled as DEEPTAU discriminators against jets ( $D_{\text{jet}}$ ), muons ( $D_\mu$ ), and electrons ( $D_e$ ).

### 4.4 Expected performance

The performance of the DEEPTAU discriminators is evaluated with the validation samples. Working points are defined to guide usage in physics analyses and to derive suitable data-to-simulation corrections. The target  $\tau_h$  identification efficiencies for the various working points

used in the wide range of physics analyses with tau leptons are presented in Table 3. The target  $\tau_h$  identification efficiencies are defined as the efficiency for genuine  $\tau_h$  in the  $H \rightarrow \tau\tau$  event sample that are reconstructed as  $\tau_h$  candidates with  $30 < p_T < 70$  GeV to pass the given discriminator. The target  $\tau_h$  identification efficiencies range from 40 to 98% for  $D_{jet}$ , from 99.5 to 99.95% for  $D_\mu$ , and from 60 to 99.5% for  $D_e$ .

Table 3: Target  $\tau_h$  identification efficiencies for the different working points defined for the three different discriminators. The target efficiencies are evaluated with the  $H \rightarrow \tau\tau$  event sample for  $\tau_h$  with  $p_T \in [30, 70]$  GeV.

	VVTight	VTight	Tight	Medium	Loose	VLoose	VVLoose	VVVLoose
$D_e$	60%	70%	80%	90%	95%	98%	99%	99.5%
$D_\mu$	—	—	99.5%	99.8%	99.9%	99.95%	—	—
$D_{jet}$	40%	50%	60%	70%	80%	90%	95%	98%

In Fig. 4, the performance of the  $D_{jet}$  discriminator is evaluated by studying the efficiencies for quark and gluon jets and genuine  $\tau_h$  to pass the discriminator and comparing it with the previously used MVA classifier. All generated and reconstructed  $\tau_h$  candidates in this figure and those that follow are required to pass  $p_T > 20$  GeV and  $|\eta| < 2.3$ , VVVLoose  $D_e$  WP and VLoose  $D_\mu$  WP. For the previously used MVA classifier, two curves are shown: The first curve corresponds to the  $\tau_h$  decay mode reconstruction as used in the previous publication and in previous physics analyses, whereas the second curve includes the additional  $\tau_h$  decay modes introduced in Section 3, leading to an overall increase of the MVA classifier performance, in particular for higher efficiency values. The efficiency is evaluated separately for the W+jets and t̄t event samples. The W+jets sample is enriched in quark jets, whereas the t̄t event sample has a larger fraction of b quark and gluon jets and has a busier event topology. The efficiencies are also evaluated separately for  $\tau_h$  candidates with  $p_T < 100$  GeV and  $p_T > 100$  GeV to test the performance in different  $p_T$  regimes. For all considered scenarios, the  $D_{jet}$  discriminator shows a large improvement of the signal efficiency at a given background efficiency compared with the previously used MVA classifier. At a given efficiency for jets to pass the discriminator, there is a relative increase in signal efficiency of more than 30% for the tightest working points and more than 10% for the loosest working points. The larger gain at high  $p_T$  is a consequence of the inclusion of additional decay modes in the  $\tau_h$  reconstruction.

The  $p_T$  dependence of the efficiency for genuine generated  $\tau_h$  with  $p_T > 20$  GeV to be reconstructed with  $p_T > 20$  GeV and to pass the  $D_{jet}$  discriminator is shown in Fig. 5. The reconstruction efficiency exceeds 80% for  $p_T > 30$  GeV and is close to 90% for  $p_T > 100$  GeV, and is mostly limited by the charged-hadron reconstruction efficiency. If decay modes with missing charged hadrons (the so-called two-prong decay modes) are excluded, the efficiency is reduced by around 10%. The efficiency to additionally pass either of the shown working points of the  $D_{jet}$  discriminator (for reconstructed  $\tau_h$  candidates without missing charged hadrons) is in line with the target  $\tau_h$  identification efficiencies listed in Table 3.

The  $D_e$  discriminator leads to a significantly improved rejection of electrons compared with the MVA discriminator, as can be inferred from Fig. 6. The efficiencies for  $\tau_h$  candidates (with  $p_T > 20$  GeV,  $|\eta| < 2.3$  and passing the VVVLoose  $D_{jet}$  and VLoose  $D_\mu$  WP) and electrons to pass the two discriminators are shown separately for  $\tau_h$  and electrons with  $20 < p_T < 100$  GeV and  $p_T > 100$  GeV. Within the range of applicability of the previously used MVA discriminator, the  $D_e$  discriminator increases the  $\tau_h$  efficiency by consistently more than 10% for a constant misidentification probability. For example, the  $\tau_h$  efficiency increases from 87 to 99% for the loosest working point of the two discriminators with an electron efficiency of around 7% for  $p_T < 100$  GeV. Besides increasing the reach in  $\tau_h$  identification efficiency, the new discriminator

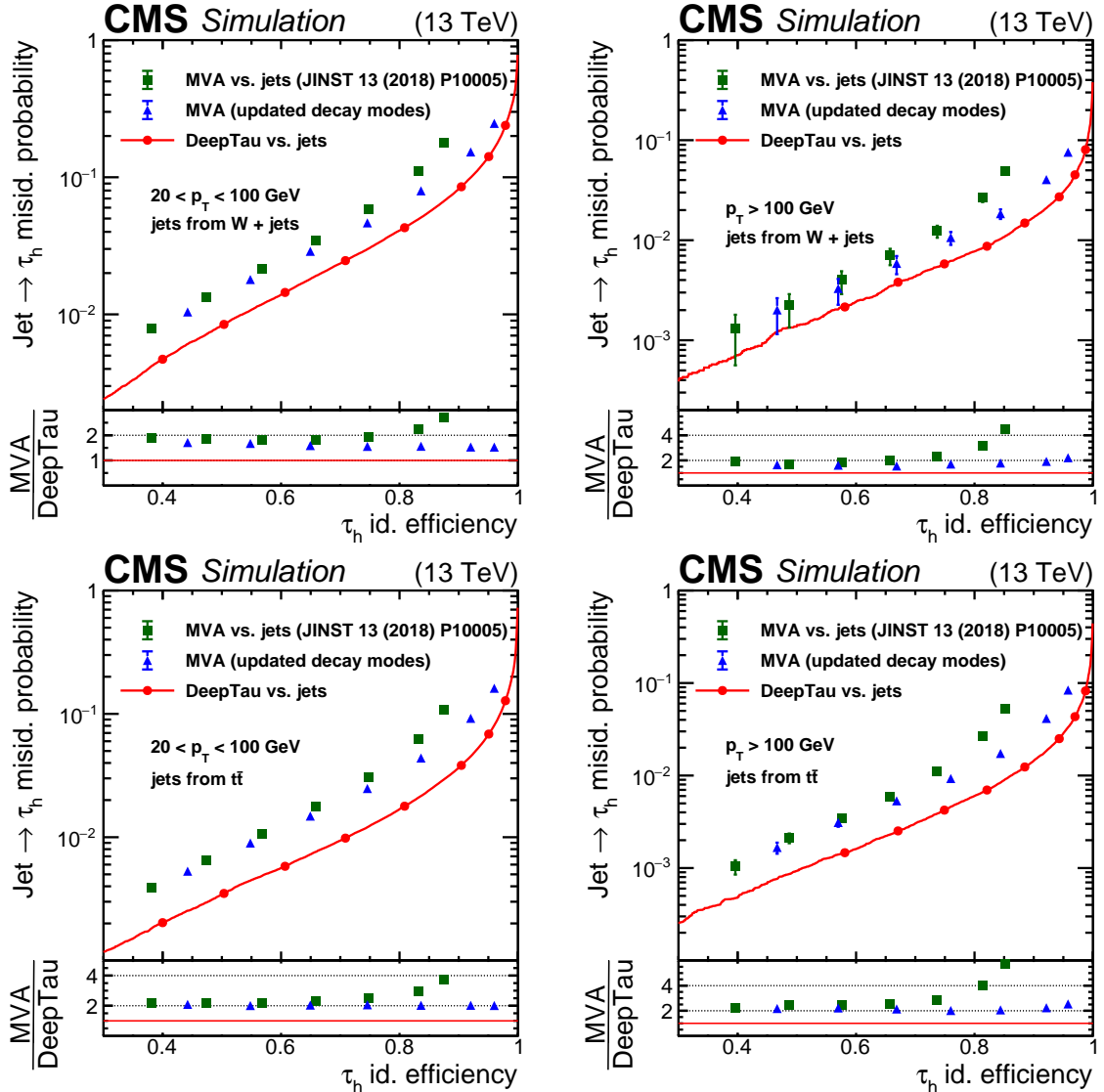


Figure 4: Efficiency for quark and gluon jets to pass different tau identification discriminators versus the efficiency for genuine  $\tau_h$ . The upper two plots are obtained with jets from the  $W+jets$  simulated sample and the lower two plots with jets from the  $t\bar{t}$  sample. The left two plots include jets and genuine  $\tau_h$  with  $p_T < 100$  GeV, whereas the right two plots include those with  $p_T > 100$  GeV. The working points are indicated as full circles. The efficiency for jets from the  $W+jets$  event sample, enriched in quark jets, to pass the discriminators is higher compared with jets from the  $t\bar{t}$  event sample, which has a larger fraction of gluon and b-quark jets. The jet efficiency for a given  $\tau_h$  efficiency is larger for jets and  $\tau_h$  with  $p_T < 100$  GeV than for those with  $p_T > 100$  GeV. Compared with the previously used MVA discriminator, the DEEPTAU discriminator reduces the jet efficiency for a given  $\tau_h$  efficiency by consistently more than a factor of 1.8, and by more at high  $\tau_h$  efficiency. The additional gain at high  $p_T$  comes from the inclusion of updated decay modes in the  $\tau_h$  reconstruction, as illustrated by the curves for the previously used MVA discriminator but including reconstructed  $\tau_h$  candidates with additional decay modes.

also provides the possibility to reject electrons with an efficiency of  $10^{-4}$  for a  $\tau_h$  efficiency of 55%. Similar, albeit slightly smaller, gains are observed for  $p_T > 100$  GeV.

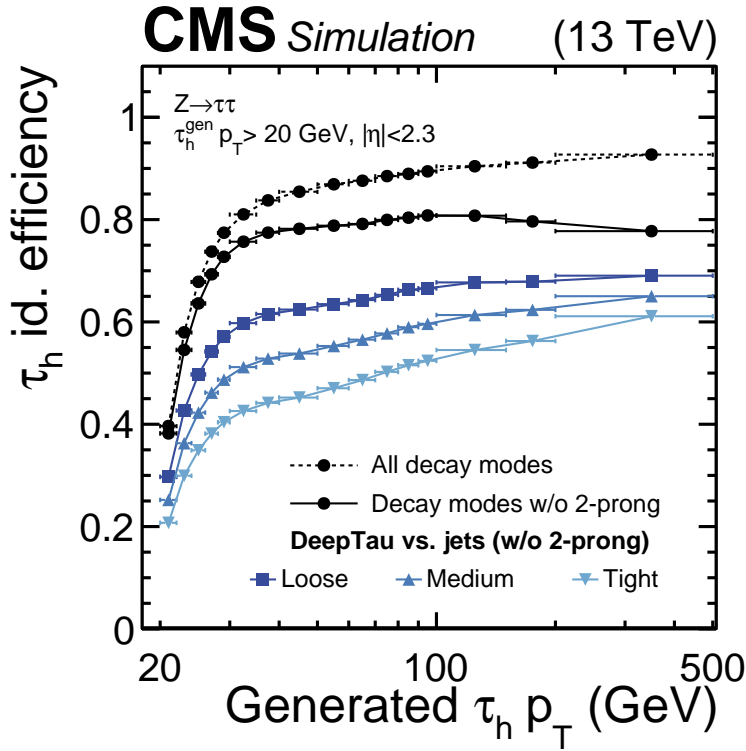


Figure 5: Efficiencies for simulated  $\tau_h$  decays with  $|\eta| < 2.3$  to pass the following reconstruction and identification requirements: to be reconstructed in any decay mode with  $p_T > 20 \text{ GeV}$  and  $|\eta| < 2.3$  (black dashed line), to be reconstructed in a decay mode except for those with missing charged hadrons (labelled “2-prong” and shown as full black line), and to be reconstructed in a decay mode except the 2-prong ones and to pass the Loose, Medium, or Tight working point of the  $D_{\text{jet}}$  discriminator (blue lines), obtained with a  $Z \rightarrow \tau\tau$  event sample. The efficiencies are shown as a function of the visible genuine  $\tau_h p_T$  obtained from simulated decay products.

Gains are also observed in terms of the discrimination of  $\tau_h$  candidates (with  $p_T > 20 \text{ GeV}$ ,  $|\eta| < 2.3$  and passing the VVVLoose  $D_{\text{jet}}$  and VVVLoose  $D_e$  WP) versus muons, as shown in Fig. 7. Compared with the cutoff-based discriminator, the  $D_\mu$  discriminator leads to an increase of the  $\tau_h$  efficiency of around 0.5% for a given prompt muon efficiency. For the  $\tau_h$  efficiency range of 99.1–99.4% addressed by the cutoff-based discriminator, the  $D_\mu$  discriminator leads to a factor of 3–10 larger prompt muon rejection, and thereby provides a significantly improved rejection of prompt muons for analyses with hadronically decaying tau leptons, while leading to only a percent-level loss of  $\tau_h$  identification efficiency.

The performance results discussed so far have been obtained with simulated samples that are consistent with the 2017 data-taking conditions. Moreover, after applying the discriminators to simulated samples that correspond to the 2016 and 2018 data-taking conditions, we see consistent performance, both in absolute terms and relative to other discriminators. Based on these findings, the discriminators  $D_e$ ,  $D_\mu$ , and  $D_{\text{jet}}$  have been recommended for all CMS analyses of LHC data at  $\sqrt{s} = 13 \text{ TeV}$ .

To summarize, the DEEPTAU discriminators against jets, electrons, and muons lead to large gains in discrimination performance against various backgrounds. The gains in  $\tau_h$  identification efficiency at a typical jet or electron efficiency used in physics analyses amount to more than 30% and 10%, respectively. Therefore, a large gain in reach is expected in physics analyses

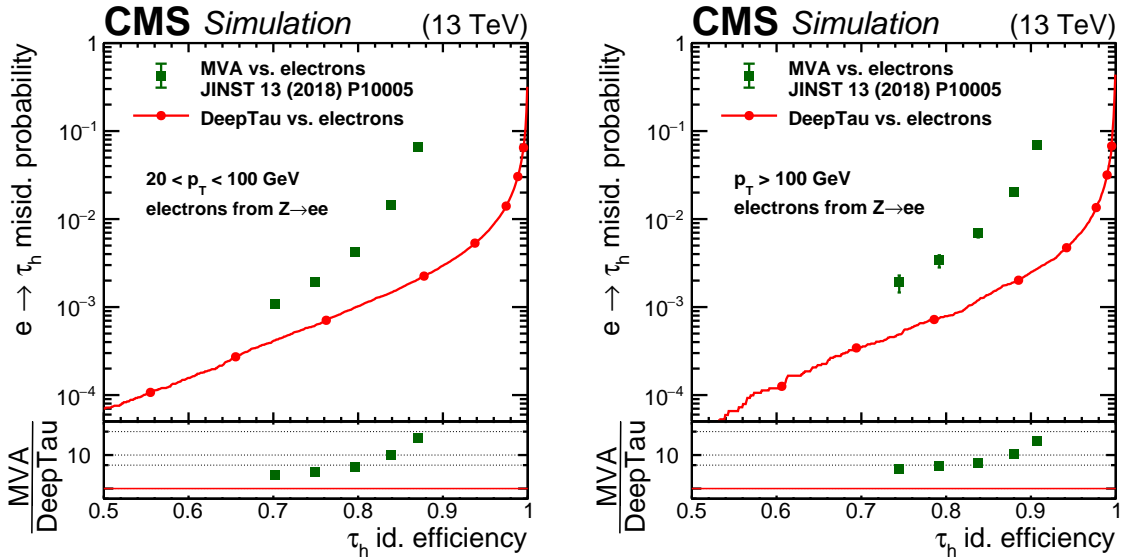


Figure 6: Efficiency for electrons versus efficiency for genuine  $\tau_h$  to pass the MVA and  $D_e$  discriminators, separately for electrons and  $\tau_h$  with  $20 < p_T < 100 \text{ GeV}$  (left) and  $p_T > 100 \text{ GeV}$  (right). Vertical bars correspond to the statistical uncertainties. The  $\tau_h$  candidates are reconstructed in one of the  $\tau_h$  decay modes without missing charged hadrons. Compared with the MVA discriminator, the  $D_e$  discriminator reduces the electron efficiency by more than a factor of two for a  $\tau_h$  efficiency of 70% and by more than a factor of 10 for  $\tau_h$  efficiencies larger than 88%. Furthermore, working points (indicated as full circles) are now provided for previously inaccessible  $\tau_h$  efficiencies larger than 90%, for a misidentification efficiency between 0.3 and 8%.

with tau leptons, in particular for final states with two  $\tau_h$  candidates. These improvements are confirmed by physics analyses that already used the DEEPTAU discriminators [72–74].

## 5 Performance with $\sqrt{s} = 13 \text{ TeV}$ data

The performance of the  $\tau_h$  reconstruction and of the DEEPTAU discriminators is validated with collision data at  $\sqrt{s} = 13 \text{ TeV}$ . The total integrated luminosity for the 2016–2018 data collected with the CMS detector and validated for use in analysis amounts to  $138 \text{ fb}^{-1}$ , of which  $36 \text{ fb}^{-1}$  were recorded in 2016,  $42 \text{ fb}^{-1}$  in 2017, and  $60 \text{ fb}^{-1}$  in 2018 [75–77]. The reconstruction and identification efficiencies for  $\tau_h$  are measured separately for the three data-taking years using a  $Z \rightarrow \tau\tau$  event sample in the  $\mu\tau_h$  final state, following methods similar to those established previously [19]. In addition, measurements are made of the misidentification efficiency with which jets, electrons, and muons are reconstructed and identified as  $\tau_h$  candidates. All of these measurements are essential ingredients for physics analyses that use  $\tau_h$  candidates.

In this paper, we present a subset of the measurements that were carried out, mostly based on the largest data set recorded in 2018. The identification efficiencies are generally measured for all working points introduced above. We discuss a subset of measurements here only for representative working points. Consistent results have been obtained for the other working points, and for the 2016 and 2017 data sets. We have not performed such efficiency measurements for the decay modes with missing charged hadrons; future analyses including these decay modes will need to derive appropriate corrections. The full set of efficiency and energy scale corrections together with their corresponding uncertainties is available for data analyses in the CMS Collaboration.

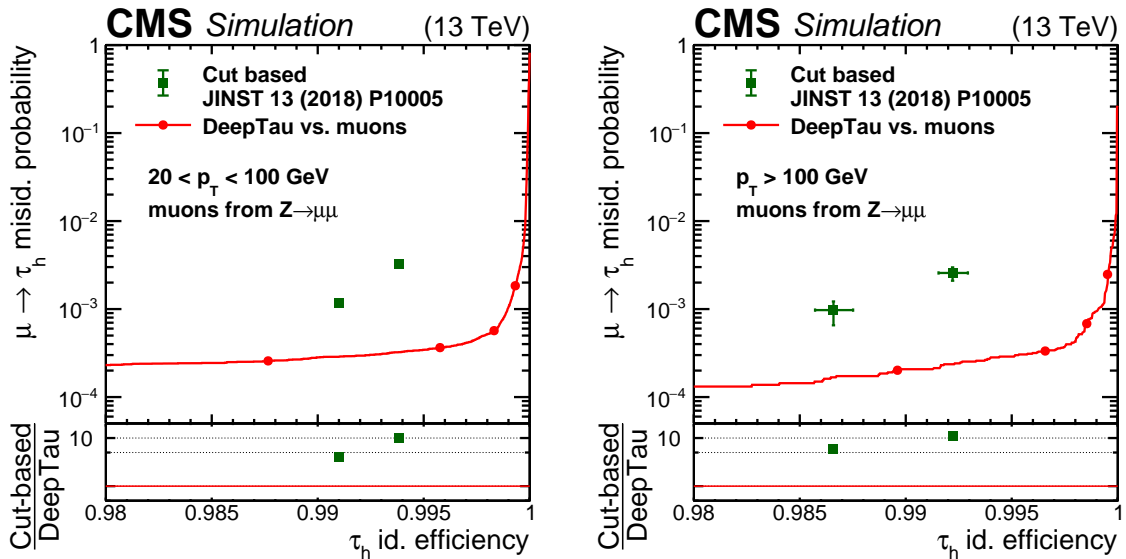


Figure 7: Efficiency for muons versus efficiency for simulated  $\tau_h$  to pass the cutoff-based and  $D_\mu$  discriminators, separately for muons and  $\tau_h$  with  $20 < p_T < 100 \text{ GeV}$  (left) and  $p_T > 100 \text{ GeV}$  (right). The four working points are indicated as full circles. Vertical bars correspond to the statistical uncertainties. In both  $p_T$  regimes, the  $D_\mu$  discriminator rejects up to a factor of 10 more muons at  $\tau_h$  efficiencies around 99%, and it leads to an increase of the  $\tau_h$  efficiency for a similar background rejection by about 0.5%.

### 5.1 Reconstruction and identification efficiency

The measurement of the  $\tau_h$  reconstruction and identification efficiencies uses a  $\mu\tau_h$  event sample that is selected in the same way as in the previous measurement [19], with the following updates. Events are recorded with a single-muon trigger with a nominal  $p_T$  threshold of 24 GeV and are required to have at least one reconstructed and isolated muon with  $p_T > 25 \text{ GeV}$ . The  $\tau_h$  candidate is required to be reconstructed with the decay mode finding algorithm, to have  $p_T > 20 \text{ GeV}$ , and to pass a given threshold on the  $D_{jet}$  discriminator. In addition, the  $\tau_h$  candidate needs to pass the VVLoose working point of the  $D_e$  discriminator and the Tight working point of the  $D_\mu$  discriminator, to reject background from muons or electrons misidentified as a  $\tau_h$  candidate. Additional criteria are applied to increase the purity of events with genuine  $\tau_h$  candidates, including a requirement on the transverse mass of the muon and  $\vec{p}_T^{\text{miss}}$  ( $\sqrt{2p_T^\mu p_T^{\text{miss}}(1 - \cos \Phi)} < 60 \text{ GeV}$ , where  $\Phi$  is the angle in the transverse plane between the muon momentum and  $\vec{p}_T^{\text{miss}}$ ) and a maximum difference in  $\eta$  between the reconstructed muon and the  $\tau_h$  candidate ( $|\Delta\eta| < 1.5$ ). The resulting dataset is enriched in  $Z \rightarrow \tau\tau$  events, with the residual contamination from other processes amounting to approximately one fifth of the total yield (Fig. 10). In addition to the  $\mu\tau_h$  event sample, a  $\mu\mu$  event sample is defined to normalize the  $Z \rightarrow \tau\tau$  event yields. This event sample is subject to the same trigger and muon selection criteria as the  $\mu\tau_h$  event sample, such that related uncertainties partially cancel in the normalization scale factor.

The efficiencies are extracted from a maximum likelihood fit to the distribution of the reconstructed visible invariant mass of the  $\mu\tau_h$  system,  $m_{\text{vis}}$ , and to the expected and observed event yields in the  $\mu\mu$  region. In the fit, the ratio of the observed and expected efficiency for a genuine  $\tau_h$  to pass the selection is incorporated as a free parameter, such that the fit yields a scale factor with respect to the simulated efficiency. All known sources of systematic uncertainties are incorporated into the fit. Uncertainties include the uncertainty in the integrated luminosity,

uncertainties in the muon trigger, identification, and isolation efficiencies, uncertainties due to the limited number of simulated events, and uncertainties in the normalizations of  $t\bar{t}$ , QCD multijet, and  $Z/\gamma^*+j$ ets background. Since the scale factors are extracted after the full event selection, they incorporate any differences between data and simulation of the full product of all reconstruction and identification efficiencies. The scale factors are extracted from the maximum likelihood fit together with their corresponding uncertainties using the asymptotic properties of the likelihood function [78].

The scale factors are extracted in different  $p_T$  bins,  $p_T \in \{[20, 25], [25, 30], [30, 35], [35, 40], [40, 50], [50, 70], >70 \text{ GeV}\}$ , to account for a possible  $p_T$  dependence of the extracted scale factors, which would affect analyses that use different minimum  $p_T$  thresholds or that analyze  $\tau_h$  final states from processes with different  $p_T$  distributions. While analyses usually use all reconstructed decay modes, except for the modes with missing charged hadrons so a parametrization in terms of decay modes is not necessary, analyses that select events using the di- $\tau_h$  trigger algorithms observe a different proportion of  $\tau_h$  candidates reconstructed in the various decay modes. This is a consequence of the dependency of  $\tau_h$  trigger efficiency on the various decay modes. Therefore, scale factors are separately determined in four bins of reconstructed decay modes ( $h^\pm$ ;  $h^\pm\pi^0$  or  $h^\pm\pi^0\pi^0$ ;  $h^\pm h^\mp h^\pm$ ; and  $h^\pm h^\mp h^\pm\pi^0$ ). These scale factors are shown in Fig. 8 for  $\tau_h p_T > 40 \text{ GeV}$ , which corresponds to the minimum recommended threshold in analyses that use events recorded with the di- $\tau_h$  trigger.

Since the reach in  $\tau_h p_T$  is limited in the  $Z \rightarrow \tau\tau$  sample, a separate off-shell W boson ( $W^*$ ) event sample is used to measure additional scale factors for  $\tau_h p_T > 100 \text{ GeV}$  in a  $\tau_h$ -plus- $p_T^{\text{miss}}$  final state without an additional hadronic jet, following closely the method discussed in Ref. [19]. The requirement of high  $\tau_h p_T$  and high  $p_T^{\text{miss}}$  combined with the hadronic jet veto leads to an event sample dominated by off-shell  $W^* \rightarrow \tau\nu_\tau$  boson decays. The events are recorded with a trigger that requires a large  $p_T^{\text{miss}}$ . The efficiencies are obtained from a maximum likelihood fit to the transverse mass distribution of the  $\tau_h$  candidate and  $p_T^{\text{miss}}$ . To constrain the fiducial  $W^*$  cross section in the signal region, a  $W^* \rightarrow \mu\nu_\mu$  control region is also included in the fit.

Figure 8 (left) shows the scale factors as a function of the reconstructed  $\tau_h$  candidate  $p_T$  separately for the Loose, Medium, and Tight working points. The plots also show the uncertainties for the  $\tau_h$  candidates with  $p_T > 40 \text{ GeV}$ , which are obtained from a constant fit up to  $p_T$  values of 500 GeV, assuming there is no statistically significant  $p_T$  dependence of the scale factors. Beyond 500 GeV, the uncertainties are enlarged because of the lack of  $\tau_h$  candidates with such high  $p_T$  values, with the uncertainty at 1000 GeV twice as large as at 500 GeV.

The  $p_T$ -dependent uncertainties in the  $\tau_h$  scale factors range from 2 to 5%. For the  $\tau_h p_T$  spectrum in the  $Z \rightarrow \tau\tau$  sample, the combined scale factor uncertainty amounts to  $\approx 2\%$ . These uncertainties are considerably smaller than in previous measurements, which reported combined uncertainties of  $\approx 6\%$  [19]. The previous measurements used the “tag-and-probe” technique [79] that only measured the identification efficiency for the discriminator under consideration and added additional uncertainties in the reconstruction efficiency from independent measurements of single charged-hadron reconstruction efficiencies. The measurement of the product of all reconstruction and identification efficiencies with a maximum likelihood fit hence represents another important improvement for physics analyses with  $\tau_h$  final states, as it leads to a considerable reduction of the systematic uncertainties related to the  $\tau_h$  reconstruction and identification.

The data-to-simulation scale factors as a function of the  $\tau_h$  decay mode are shown in Fig. 8 (right) for  $\tau_h p_T > 40 \text{ GeV}$  for the three data-taking years (2016, 2017, and 2018). The scale

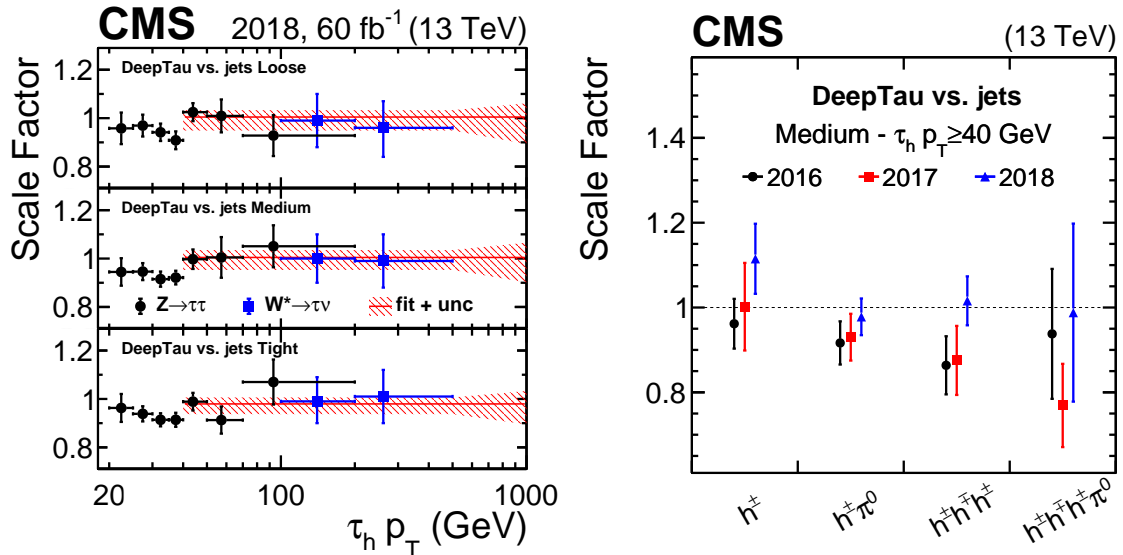


Figure 8: Data-to-simulation scale factors for genuine  $\tau_h$  to be reconstructed as  $\tau_h$  candidates and to pass the Loose, Medium, and Tight working points of the  $D_{jet}$  discriminator as a function of the  $\tau_h$  candidate  $p_T$  (left). Vertical bars correspond to the combined statistical and systematic uncertainties in the individual scale factors. The red hatched bands indicate the uncertainties for  $p_T > 40$  GeV, obtained from a combination of the individual measurements. The right plot shows the data-to-simulation scale factors for the  $\tau_h$  candidates with  $p_T > 40$  GeV to pass the Medium  $D_{jet}$  working point as a function of reconstructed  $\tau_h$  decay mode. The efficiencies are obtained with 2018 data and the according simulated events using a likelihood fit to the distribution of the reconstructed  $m_{vis}(\mu, \tau_h)$ . The scale factors are shown separately for data taken in 2016, 2017, and 2018 (and the corresponding simulated events) and for the four main  $\tau_h$  decay modes.

factors are generally a bit smaller than one but consistent with unity within 10% (20% for the  $\tau_h$  candidates reconstructed in the  $h^\pm h^\mp h^\pm \pi^0$  decay mode). The scale factors below one can be traced back to different origins, including the imperfect modelling of hadronization and an imperfect simulation of the detector alignment and track hit reconstruction efficiencies.

## 5.2 The $\tau_h$ energy scale

The  $\tau_h$  energy scale is obtained from the same  $\mu\tau_h$  event samples as the scale factors discussed in the previous section, following the same method described in previous publications [19]. For the main measurement discussed here,  $\tau_h$  candidates are required to pass the Medium working point of the  $D_{jet}$  discriminator. Consistent results are obtained with cross-check measurements for various working points of the  $D_{jet}$  discriminator. To improve the a priori data-simulation agreement, scale factors as described in the previous section are already applied to simulated samples with  $\tau_h$  final states.

Two different observables are used to measure the  $\tau_h$  energy scale: the  $\mu\tau_h$  invariant mass ( $m_{vis}$ ) and the reconstructed  $\tau_h$  mass ( $m(\tau_h)$ ). For  $\tau_h$  candidates reconstructed in the  $h^\pm$  decay mode,  $m(\tau_h)$  is constant, so the measurement is only performed with the  $m_{vis}$  observable.

Simulated templates of the  $m_{vis}$  and  $m(\tau_h)$  distributions are created for  $\tau_h$  energy scale shifts between  $\pm 3\%$  in steps of 0.2%. For each shift, a maximum likelihood fit is performed, using the combined expectation from the  $Z \rightarrow \tau\tau$  in the  $\mu\tau_h$  final state and the background events, using the set of systematic uncertainties discussed above. The observed value of the  $\tau_h$  energy scale

shift is obtained from the distribution of the likelihood ratio together with the corresponding uncertainty.

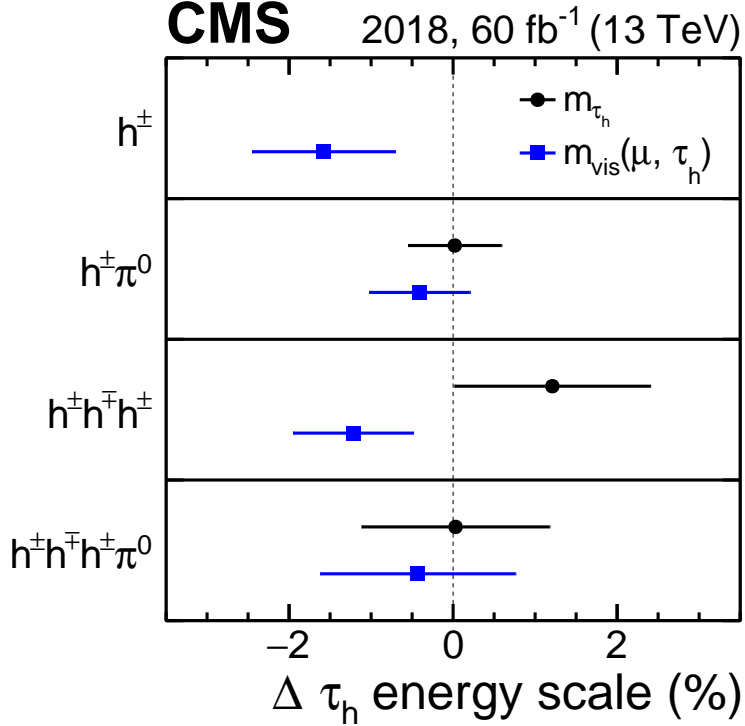


Figure 9: Relative difference between  $\tau_h$  energy obtained in data and simulated events for the four main reconstructed  $\tau_h$  decay modes for the 2018 data set. The results are obtained from fits to the distribution of either the reconstructed  $m_{\text{vis}}(\mu, \tau_h)$  (blue lines) or  $m_{\tau_h}$  (black lines). The horizontal bars represent the uncertainties in the measurements. The measured values are consistent with no shift of the  $\tau_h$  energy scale between data and simulation, with the largest difference amounting to 1.5 standard deviations.

The resulting relative differences between the  $\tau_h$  energy scale in data and simulation are shown in Fig. 9 separately for the two different measurements. The relative difference is given as a correction, in percent, to a unit multiplicative factor applied to the  $\tau_h$  four-momentum in the simulation. The results obtained with the two methods are consistent with each other, and the  $\tau_h$  energy scale shifts are consistent with no data-simulation differences, with the largest difference amounting to 1.5 standard deviations. The relative uncertainties range from 0.6% for the  $h^\pm\pi^0$  and  $h^\pm h^\mp h^\pm$  decay modes to 0.8% for the  $h^\pm$  mode.

To validate the extracted scale factors and to illustrate the distributions used for the extraction of the scale factors and the  $\tau_h$  energy corrections, distributions of  $m_{\text{vis}}$  and  $m(\tau_h)$  are investigated, requiring the  $\tau_h$  to pass the Tight working point of the  $D_{\text{jet}}$  discriminator (Fig. 10). These distributions are obtained from a maximum likelihood fit to the  $\mu\tau$  data, applying the same selection used in the extraction of the scale factors. This fit incorporates the derived scale factors and energy corrections with their uncertainties, together with the full set of systematic uncertainties used in the scale factor extractions. In the fit to data, the  $Z \rightarrow \tau\tau$  normalization is a freely floating parameter. Data and predictions agree within the uncertainties, indicating that the derived scale factors and energy corrections lead to a good and complete description of the data, including the description of the different  $\tau_h$  decay modes.

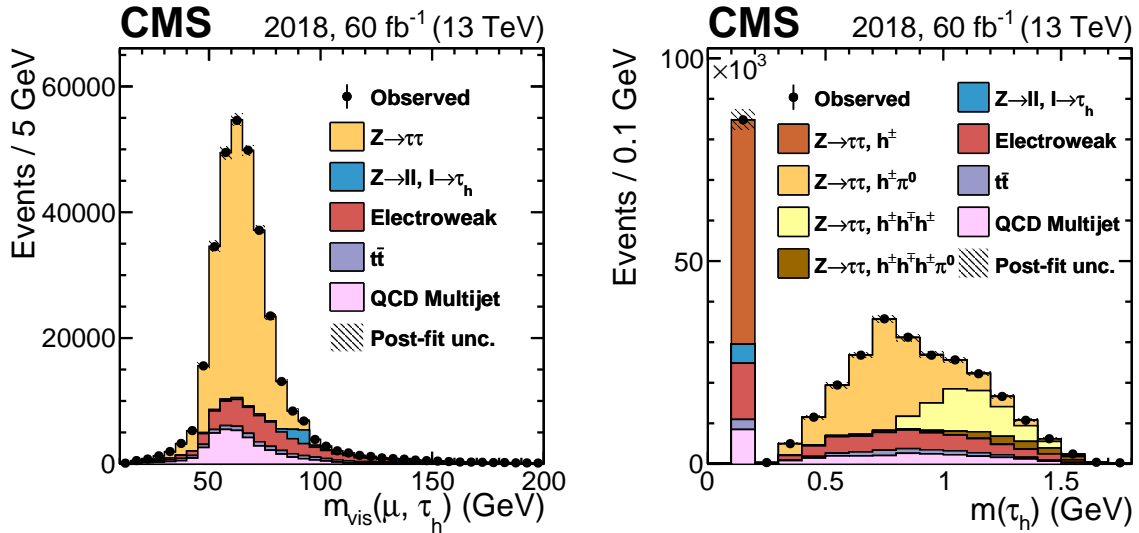


Figure 10: Distribution of the reconstructed visible invariant mass of the  $\mu\tau_h$  system,  $m_{\text{vis}}(\mu, \tau_h)$  (left) and of the visible invariant  $\tau_h$  mass (right). Vertical bars correspond to the statistical uncertainties. The event selection corresponds to the one in the measurement of the  $\tau_h$  reconstruction and identification efficiencies and uses the Tight working point of the  $D_{\text{jet}}$  discriminator. The distributions incorporate all measured scale factors and energy corrections and are scaled to the outcome of a maximum likelihood to the observed data with the  $Z \rightarrow \tau\tau$  contribution freely floating. The electroweak background combines contributions from single top quark, diboson, and  $W$ -jets processes as well as  $Z(\rightarrow \tau\tau)$ -jets events where the reconstructed  $\tau_h$  originates from a jet misidentified as a  $\tau_h$  candidate instead of one of the produced tau leptons. In the  $m(\tau_h)$  distribution, the  $Z \rightarrow \tau\tau$  contributions are shown separately for the different  $\tau_h$  decay modes.

### 5.3 Lepton and jet misidentification efficiencies

The efficiencies for electrons, muons, and jets to pass the respective DEEPTAU discriminators are measured with dedicated event samples, following closely the measurements explained in detail in Ref. [19]. The efficiencies for electrons and muons to be reconstructed and misidentified as  $\tau_h$  candidates are measured with  $Z \rightarrow \ell\ell$  events ( $\ell \in \{\text{e}, \mu\}$ ) where one  $\ell$  is misreconstructed as a  $\tau_h$  candidate; the event is reconstructed as an  $\ell\tau_h$  final state. The efficiencies are extracted with the tag-and-probe method, where  $\ell$  candidates that pass a given working point of the  $D_\mu$  or  $D_e$  discriminator end up in the pass region and those that do not pass in the fail region. A maximum likelihood fit is performed to obtain the efficiencies. The distribution used in the pass region is the invariant  $\ell\tau_h$  mass ( $m_{\text{vis}}$ ), whereas the fail region is included as a single bin. Similar to the extraction of the  $\tau_h$  efficiencies, all relevant uncertainties are included in the maximum likelihood fit. To reject background from jets reconstructed as  $\tau_h$  candidates, the candidates are also required to pass the Medium working point of the  $D_{\text{jet}}$  discriminator. An additional parameter is introduced in the fit that scales the contributions in the pass and fail regions simultaneously and corresponds to the scale factor for the efficiency to pass the  $D_{\text{jet}}$  discriminator. This approach is based on the assumption that the probability for electrons or muons to pass the  $D_{\text{jet}}$  discriminator is independent of the probability to pass the  $D_e$  or  $D_\mu$  discriminator. Another parameter is introduced for electrons misreconstructed as  $\tau_h$  candidates that allows for a shifted energy scale.

The  $e\tau_h$  events for the measurement of the scale factors for electrons to pass different working points of the  $D_e$  discriminator are recorded with a single-electron trigger with a  $p_T$  threshold of

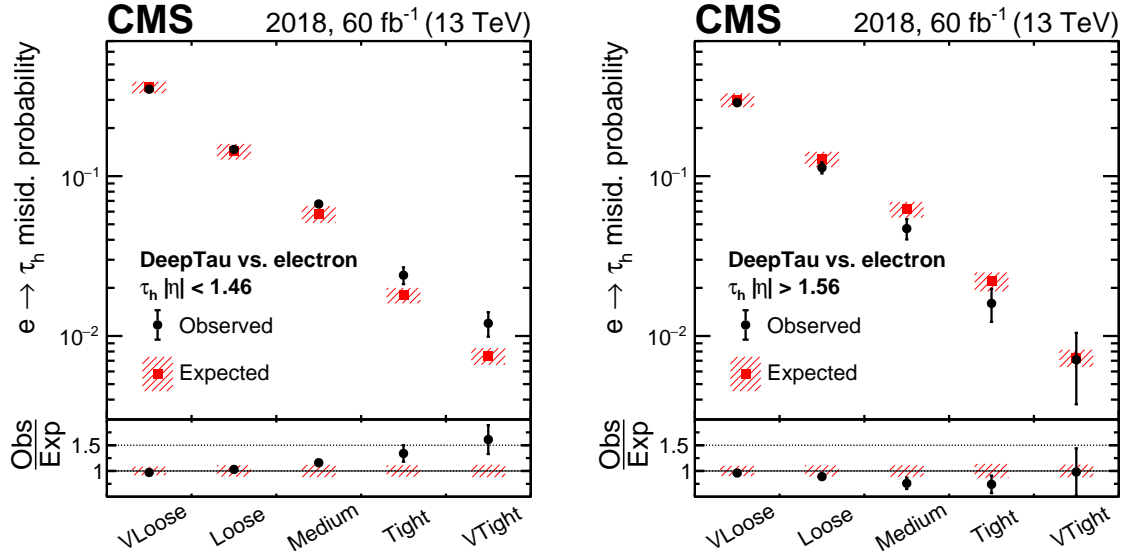


Figure 11: Observed and expected efficiencies for electrons to pass different  $D_e$  working points. Vertical bars correspond to the combined statistical and systematic uncertainties in the individual scale factors. The electrons are required to be reconstructed as a  $\tau_h$  candidate and to pass the medium  $D_{jet}$  working point. The efficiencies are shown separately for electrons with  $|\eta| < 1.46$  (left), corresponding to the ECAL barrel region, and  $|\eta| > 1.56$  (right), corresponding to the ECAL endcap regions.

35 GeV. The efficiencies for electrons to pass the different working points in data and simulated events as well as the ratio of the efficiencies are shown in Fig. 11. The efficiencies are derived separately in the ECAL barrel region ( $|\eta| < 1.46$ ) and the ECAL endcap region ( $|\eta| > 1.56$ ). The observed and expected efficiencies agree within a few percent for the Loose and VLoose working points in the barrel and within 11% in the endcap region. For tighter working points, scale factors are obtained that are significantly different from one and that are generally greater than one in the barrel, with a maximum scale factor of  $1.61 \pm 0.28$  for the VTight working point, and smaller in the endcap.

The  $\mu\tau_h$  events for the measurement of the scale factors for muons to be misreconstructed and misidentified as  $\tau_h$  candidates are recorded with a single-muon trigger with a threshold of 27 GeV. The leading muon is required to have  $p_T > 28$  GeV, and the transverse mass of the muon and  $\vec{p}_T^{\text{miss}}$  is required to be smaller than 30 GeV. The resulting data-to-simulation scale factors are extracted from a fit to the  $m_{\text{vis}}$  distribution and are shown in Fig. 12. The scale factors are shown separately for the Loose and Tight working points, and for five different bins in  $|\eta|$ . Although the scale factors are consistent with each other for the different working points and consistent with unity for four of the  $|\eta|$  bins, they differ significantly from one for  $|\eta| > 1.7$ . As a result of the high rejection power of  $D_\mu$ , muons that are not discarded belong to atypical regions of the phase space, far from the bulk of the distributions. For such uncommon muons, we observe that the simulation does not model the data well, especially for observables related to the muon track quality at large  $|\eta|$ ; this is compatible with being the cause of the sizeable data-to-simulation difference at  $|\eta| > 1.7$ . The large  $D_\mu$  scale factors at  $|\eta| > 1.7$  have no notable impact on physics analyses because of the small probability for muons to pass any  $D_\mu$  working point and the limited extent of the region presenting large data-to-simulation differences.

For a measurement of the efficiency for jets to pass the  $D_{jet}$  discriminator, events are selected that are consistent with a  $W(\rightarrow \mu\nu_\mu)$ +jet topology. Similar to the previously discussed mea-

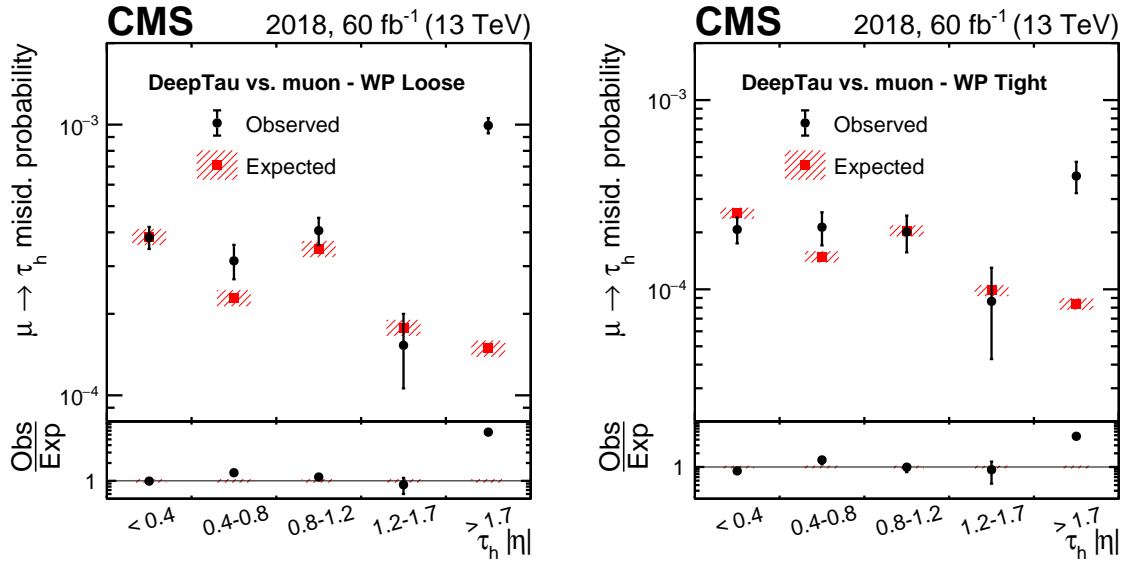


Figure 12: Observed and expected efficiencies for muons to pass the loose (left) and tight (right)  $D_\mu$  working points. Vertical bars correspond to the combined statistical and systematic uncertainties in the individual scale factors. The muons are required to be reconstructed as  $\tau_h$  candidates and to pass the Medium  $D_{\text{jet}}$  working point. The efficiencies are shown for several bins in  $|\eta|$ .

surement, the events are recorded with a single-muon trigger with a  $p_T$  threshold of 27 GeV, and the reconstructed muon is required to have  $p_T > 28$  GeV. Furthermore, there must be exactly one central jet with  $p_T > 20$  GeV and  $|\eta| < 2.3$ , and events with additional reconstructed muons or a reconstructed electron passing loose identification criteria are rejected. To select a pure sample of W+jets events, the transverse mass of the muon and  $p_T^{\text{miss}}$  is required to be greater than 60 GeV. The reconstructed jet serves as a probe for the measurement of the jet-to- $\tau_h$  misidentification efficiency. The efficiencies for jets to be reconstructed as  $\tau_h$  candidates and to pass the Loose and Tight  $D_{\text{jet}}$  working points are shown in Fig. 13 as a function of reconstructed jet  $p_T$ . In the measurement of the efficiency, background events with genuine  $\tau_h$  candidates are subtracted. The observed and expected efficiencies agree within the uncertainties.

## 6 Summary

A new algorithm has been introduced to discriminate hadronic tau lepton decays ( $\tau_h$ ) against jets, electrons, and muons. The algorithm is based on a deep neural network and combines fully connected and convolutional layers. As input, the algorithm combines information from individual reconstructed particles near the  $\tau_h$  axis with information about the reconstructed  $\tau_h$  candidate and other high-level variables. In addition, an improved  $\tau_h$  reconstruction algorithm is introduced that increases the overall efficiency of the reconstruction by explicitly considering the  $\tau_h$  decay mode with three charged hadrons and a neutral pion, and by applying looser quality criteria for the charged hadrons in the case of three-prong  $\tau_h$  decays. The performance of the new  $\tau_h$  identification and reconstruction algorithms significantly improves over the previously used algorithms, in particular in terms of discrimination against the background from jets and electrons. For a given jet rejection level, the efficiency for genuine  $\tau_h$  candidates increases by 10–30%. Similarly, the efficiency for genuine  $\tau_h$  candidates to pass the discriminator against electrons increases by 14% for the loosest working point that is employed in many analyses. Following its superior performance, CMS physics analyses with tau leptons will sig-

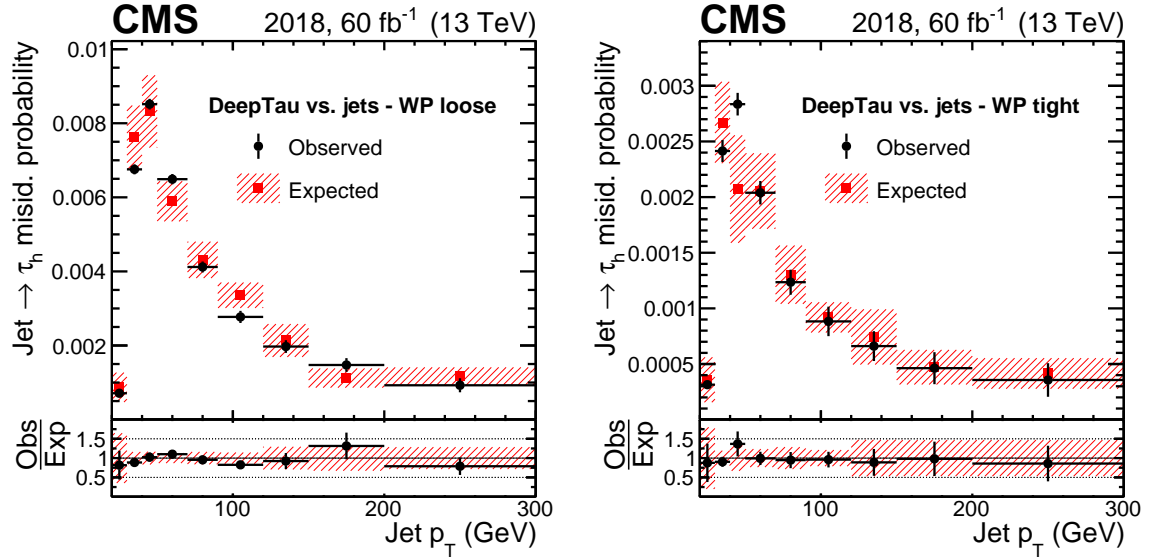


Figure 13: Observed and expected efficiencies for quark and gluon jets with  $|\eta| < 2.3$  to be reconstructed as  $\tau_h$  candidates with  $p_T > 20\text{ GeV}$  and to pass the loose (left) and tight (right)  $D_{\text{jet}}$  working points. The efficiencies are shown as a function of reconstructed jet  $p_T$  and are obtained with data recorded in 2018 and the corresponding simulated events. The shaded uncertainty band includes contributions from the limited number of simulated events and from uncertainties in the jet energy scale and the  $p_T^{\text{miss}}$  description. Besides the statistical uncertainty in the observed events, the error bars in the ratio of data to simulation also include uncertainties from the subtraction of events with genuine  $\tau_h$  candidates, electrons, or muons. The efficiency first rises with  $p_T$  near the 20 GeV threshold because it becomes more likely for a jet to give rise to a reconstructed  $\tau_h$  candidate that passes this threshold. For higher  $p_T$ , the particle multiplicity in a quark or gluon jet increases with  $p_T$ . Therefore, the jets become easier to distinguish from genuine  $\tau_h$  candidates and the probability for quark or gluon jets to pass the  $D_{\text{jet}}$  discriminator decreases with  $p_T$ .

nificantly increase their sensitivities when using the new algorithm. The superior performance of the algorithm is validated with collision data. The observed efficiencies for genuine  $\tau_h$  jets, and electrons to be identified as  $\tau_h$  typically agree within 10% with the expected efficiencies from simulated events. The agreement is similar to the one observed with previous algorithms and confirms the improvements.

## Acknowledgments

We congratulate our colleagues in the CERN accelerator departments for the excellent performance of the LHC and thank the technical and administrative staffs at CERN and at other CMS institutes for their contributions to the success of the CMS effort. In addition, we gratefully acknowledge the computing centers and personnel of the Worldwide LHC Computing Grid and other centers for delivering so effectively the computing infrastructure essential to our analyses. Finally, we acknowledge the enduring support for the construction and operation of the LHC, the CMS detector, and the supporting computing infrastructure provided by the following funding agencies: BMBWF and FWF (Austria); FNRS and FWO (Belgium); CNPq, CAPES, FAPERJ, FAPERGS, and FAPESP (Brazil); MES and BNSF (Bulgaria); CERN; CAS, MoST, and NSFC (China); MINCIENCIAS (Colombia); MSES and CSF (Croatia); RIF (Cyprus); SENESCYT (Ecuador); MoER, ERC PUT and ERDF (Estonia); Academy of Finland, MEC, and HIP (Fin-

land); CEA and CNRS/IN2P3 (France); BMBF, DFG, and HGF (Germany); GSRI (Greece); NK-FIA (Hungary); DAE and DST (India); IPM (Iran); SFI (Ireland); INFN (Italy); MSIP and NRF (Republic of Korea); MES (Latvia); LAS (Lithuania); MOE and UM (Malaysia); BUAP, CINVESTAV, CONACYT, LNS, SEP, and UASLP-FAI (Mexico); MOS (Montenegro); MBIE (New Zealand); PAEC (Pakistan); MSHE and NSC (Poland); FCT (Portugal); JINR (Dubna); MON, RosAtom, RAS, RFBR, and NRC KI (Russia); MESTD (Serbia); MCIN/AEI and PCTI (Spain); MOSTR (Sri Lanka); Swiss Funding Agencies (Switzerland); MST (Taipei); ThEPCenter, IPST, STAR, and NSTDA (Thailand); TUBITAK and TAEK (Turkey); NASU (Ukraine); STFC (United Kingdom); DOE and NSF (USA).

Individuals have received support from the Marie-Curie program and the European Research Council and Horizon 2020 Grant, contract Nos. 675440, 724704, 752730, 758316, 765710, 824093, 884104, and COST Action CA16108 (European Union); the Leventis Foundation; the Alfred P. Sloan Foundation; the Alexander von Humboldt Foundation; the Belgian Federal Science Policy Office; the Fonds pour la Formation à la Recherche dans l'Industrie et dans l'Agriculture (FRIBA-Belgium); the Agentschap voor Innovatie door Wetenschap en Technologie (IWT-Belgium); the F.R.S.-FNRS and FWO (Belgium) under the "Excellence of Science – EOS" – be.h project n. 30820817; the Beijing Municipal Science & Technology Commission, No. Z191100007219010; the Ministry of Education, Youth and Sports (MEYS) of the Czech Republic; the Deutsche Forschungsgemeinschaft (DFG), under Germany's Excellence Strategy – EXC 2121 "Quantum Universe" – 390833306, and under project number 400140256 - GRK2497; the Lendület ("Momentum") Program and the János Bolyai Research Scholarship of the Hungarian Academy of Sciences, the New National Excellence Program ÚNKP, the NK-FIA research grants 123842, 123959, 124845, 124850, 125105, 128713, 128786, and 129058 (Hungary); the Council of Science and Industrial Research, India; the Latvian Council of Science; the Ministry of Science and Higher Education and the National Science Center, contracts Opus 2014/15/B/ST2/03998 and 2015/19/B/ST2/02861 (Poland); the Fundação para a Ciência e a Tecnologia, grant CEECIND/01334/2018 (Portugal); the National Priorities Research Program by Qatar National Research Fund; the Ministry of Science and Higher Education, projects no. 0723-2020-0041 and no. FSWW-2020-0008, and the Russian Foundation for Basic Research, project No.19-42-703014 (Russia); MCIN/AEI/10.13039/501100011033, ERDF "a way of making Europe", and the Programa Estatal de Fomento de la Investigación Científica y Técnica de Excelencia María de Maeztu, grant MDM-2017-0765 and Programa Severo Ochoa del Principado de Asturias (Spain); the Stavros Niarchos Foundation (Greece); the Rachadapisek Sompot Fund for Postdoctoral Fellowship, Chulalongkorn University and the Chulalongkorn Academic into Its 2nd Century Project Advancement Project (Thailand); the Kavli Foundation; the Nvidia Corporation; the SuperMicro Corporation; the Welch Foundation, contract C-1845; and the Weston Havens Foundation (USA).

## References

- [1] CMS Collaboration, "Observation of the Higgs boson decay to a pair of  $\tau$  leptons with the CMS detector", *Phys. Lett. B* **779** (2018) 283,  
[doi:10.1016/j.physletb.2018.02.004](https://doi.org/10.1016/j.physletb.2018.02.004), arXiv:1708.00373.
- [2] CMS Collaboration, "Search for Higgs boson pair production in events with two bottom quarks and two tau leptons in proton–proton collisions at  $\sqrt{s} = 13$  TeV", *Phys. Lett. B* **778** (2018) 101, [doi:10.1016/j.physletb.2018.01.001](https://doi.org/10.1016/j.physletb.2018.01.001), arXiv:1707.02909.

- [3] ATLAS Collaboration, “Cross-section measurements of the Higgs boson decaying into a pair of  $\tau$ -leptons in proton-proton collisions at  $\sqrt{s} = 13$  TeV with the ATLAS detector”, *Phys. Rev. D* **99** (2019) 072001, doi:10.1103/PhysRevD.99.072001, arXiv:1811.08856.
- [4] ATLAS Collaboration, “Search for resonant and non-resonant Higgs boson pair production in the  $b\bar{b}\tau^+\tau^-$  decay channel in pp collisions at  $\sqrt{s} = 13$  TeV with the ATLAS detector”, *Phys. Rev. Lett.* **121** (2018) 191801, doi:10.1103/PhysRevLett.121.191801, arXiv:1808.00336. [Erratum: doi:10.1103/PhysRevLett.122.089901].
- [5] ATLAS Collaboration, “Test of CP invariance in vector-boson fusion production of the Higgs boson in the  $H \rightarrow \tau\tau$  channel in proton–proton collisions at  $\sqrt{s} = 13$  TeV with the ATLAS detector”, *Phys. Lett. B* **805** (2020) 135426, doi:10.1016/j.physletb.2020.135426, arXiv:2002.05315.
- [6] CMS Collaboration, “Search for additional neutral MSSM Higgs bosons in the  $\tau\tau$  final state in proton-proton collisions at  $\sqrt{s} = 13$  TeV”, *JHEP* **09** (2018) 007, doi:10.1007/JHEP09(2018)007, arXiv:1803.06553.
- [7] ATLAS Collaboration, “Search for charged Higgs bosons decaying via  $H^\pm \rightarrow \tau^\pm \nu_\tau$  in the  $\tau + \text{jets}$  and  $\tau + \text{lepton}$  final states with  $36 \text{ fb}^{-1}$  of pp collision data recorded at  $\sqrt{s} = 13$  TeV with the ATLAS experiment”, *JHEP* **09** (2018) 139, doi:10.1007/JHEP09(2018)139, arXiv:1807.07915.
- [8] CMS Collaboration, “Search for an exotic decay of the Higgs boson to a pair of light pseudoscalars in the final state with two b quarks and two  $\tau$  leptons in proton-proton collisions at  $\sqrt{s} = 13$  TeV”, *Phys. Lett. B* **785** (2018) 462, doi:10.1016/j.physletb.2018.08.057, arXiv:1805.10191.
- [9] CMS Collaboration, “Search for a heavy pseudoscalar Higgs boson decaying into a 125 GeV Higgs boson and a Z boson in final states with two tau and two light leptons at  $\sqrt{s} = 13$  TeV”, *JHEP* **03** (2020) 065, doi:10.1007/JHEP03(2020)065, arXiv:1910.11634.
- [10] CMS Collaboration, “Search for lepton flavour violating decays of a neutral heavy Higgs boson to  $\mu\tau$  and  $e\tau$  in proton-proton collisions at  $\sqrt{s} = 13$  TeV”, *JHEP* **03** (2020) 103, doi:10.1007/JHEP03(2020)103, arXiv:1911.10267.
- [11] CMS Collaboration, “Search for a low-mass  $\tau^+\tau^-$  resonance in association with a bottom quark in proton-proton collisions at  $\sqrt{s} = 13$  TeV”, *JHEP* **05** (2019) 210, doi:10.1007/JHEP05(2019)210, arXiv:1903.10228.
- [12] CMS Collaboration, “Search for charged Higgs bosons in the  $H^\pm \rightarrow \tau^\pm \nu_\tau$  decay channel in proton-proton collisions at  $\sqrt{s} = 13$  TeV”, *JHEP* **07** (2019) 142, doi:10.1007/JHEP07(2019)142, arXiv:1903.04560.
- [13] ATLAS Collaboration, “Search for heavy Higgs bosons decaying into two tau leptons with the ATLAS detector using pp collisions at  $\sqrt{s} = 13$  TeV”, *Phys. Rev. Lett.* **125** (2020) 051801, doi:10.1103/PhysRevLett.125.051801, arXiv:2002.12223.
- [14] CMS Collaboration, “Search for direct pair production of supersymmetric partners to the  $\tau$  lepton in proton-proton collisions at  $\sqrt{s} = 13$  TeV”, *Eur. Phys. J. C* **80** (2020) 189, doi:10.1140/epjc/s10052-020-7739-7, arXiv:1907.13179.

- [15] CMS Collaboration, “Search for heavy neutrinos and third-generation leptoquarks in hadronic states of two  $\tau$  leptons and two jets in proton-proton collisions at  $\sqrt{s} = 13$  TeV”, *JHEP* **03** (2019) 170, doi:10.1007/JHEP03(2019)170, arXiv:1811.00806.
- [16] ATLAS Collaboration, “Searches for third-generation scalar leptoquarks in  $\sqrt{s} = 13$  TeV pp collisions with the ATLAS detector”, *JHEP* **06** (2019) 144, doi:10.1007/JHEP06(2019)144, arXiv:1902.08103.
- [17] CMS Collaboration, “Performance of tau-lepton reconstruction and identification in CMS”, *JINST* **7** (2012) P01001, doi:10.1088/1748-0221/7/01/P01001, arXiv:1109.6034.
- [18] CMS Collaboration, “Reconstruction and identification of  $\tau$  lepton decays to hadrons and  $\nu_\tau$  at CMS”, *JINST* **11** (2016) P01019, doi:10.1088/1748-0221/11/01/P01019, arXiv:1510.07488.
- [19] CMS Collaboration, “Performance of reconstruction and identification of  $\tau$  leptons decaying to hadrons and  $\nu_\tau$  in pp collisions at  $\sqrt{s} = 13$  TeV”, *JINST* **13** (2018) P10005, doi:10.1088/1748-0221/13/10/P10005, arXiv:1809.02816.
- [20] ATLAS Collaboration, “Identification and energy calibration of hadronically decaying tau leptons with the ATLAS experiment in pp collisions at  $\sqrt{s} = 8$  TeV”, *Eur. Phys. J. C* **75** (2015) 303, doi:10.1140/epjc/s10052-015-3500-z, arXiv:1412.7086.
- [21] ATLAS Collaboration, “Reconstruction of hadronic decay products of tau leptons with the ATLAS experiment”, *Eur. Phys. J. C* **76** (2016) 295, doi:10.1140/epjc/s10052-016-4110-0, arXiv:1512.05955.
- [22] Y. LeCun et al., “Backpropagation applied to handwritten zip code recognition”, *Neural Comput.* **1** (1989) 541, doi:10.1162/neco.1989.1.4.541.
- [23] Y. LeCun et al., “Handwritten digit recognition with a back-propagation network”, in *Advances in Neural Information Processing Systems 2*, p. 396. Morgan Kaufmann, 1990.
- [24] Y. Lecun, L. Bottou, Y. Bengio, and P. Haffner, “Gradient-based learning applied to document recognition”, *Proc. IEEE* **86** (1998) 2278, doi:10.1109/5.726791.
- [25] V. Innocente, Y. F. Wang, and Z. P. Zhang, “Identification of tau decays using a neural network”, *Nucl. Instrum. Meth. A* **323** (1992) 647, doi:10.1016/0168-9002(92)90011-R.
- [26] ATLAS Collaboration, “Identification of hadronic tau lepton decays using neural networks in the ATLAS experiment”, ATLAS PUB Note ATL-PHYS-PUB-2019-033, 2019.
- [27] CMS Collaboration, “Identification of heavy-flavour jets with the CMS detector in pp collisions at 13 TeV”, *JINST* **13** (2018) P05011, doi:10.1088/1748-0221/13/05/P05011, arXiv:1712.07158.
- [28] ATLAS Collaboration, “Identification of jets containing b-hadrons with recurrent neural networks at the ATLAS experiment”, ATLAS PUB Note ATL-PHYS-PUB-2017-003, 2017.
- [29] ATLAS Collaboration, “Deep sets based neural networks for impact parameter flavour tagging in ATLAS”, ATLAS PUB Note ATL-PHYS-PUB-2020-014, 2020.

- [30] E. Bols et al., “Jet flavour classification using DEEPJET”, *JINST* **15** (2020) P12012, doi:[10.1088/1748-0221/15/12/P12012](https://doi.org/10.1088/1748-0221/15/12/P12012), arXiv:[2008.10519](https://arxiv.org/abs/2008.10519).
- [31] CMS Collaboration, “Identification of heavy, energetic, hadronically decaying particles using machine-learning techniques”, *JINST* **15** (2020) P06005, doi:[10.1088/1748-0221/15/06/P06005](https://doi.org/10.1088/1748-0221/15/06/P06005), arXiv:[2004.08262](https://arxiv.org/abs/2004.08262).
- [32] HEPData record for this analysis, 2022. doi:[10.17182/hepdata.116281](https://doi.org/10.17182/hepdata.116281).
- [33] CMS Collaboration, “The CMS experiment at the CERN LHC”, *JINST* **3** (2008) S08004, doi:[10.1088/1748-0221/3/08/S08004](https://doi.org/10.1088/1748-0221/3/08/S08004).
- [34] CMS Collaboration, “Particle-flow reconstruction and global event description with the CMS detector”, *JINST* **12** (2017) P10003, doi:[10.1088/1748-0221/12/10/P10003](https://doi.org/10.1088/1748-0221/12/10/P10003), arXiv:[1706.04965](https://arxiv.org/abs/1706.04965).
- [35] M. Cacciari, G. P. Salam, and G. Soyez, “The anti- $k_T$  jet clustering algorithm”, *JHEP* **04** (2008) 063, doi:[10.1088/1126-6708/2008/04/063](https://doi.org/10.1088/1126-6708/2008/04/063), arXiv:[0802.1189](https://arxiv.org/abs/0802.1189).
- [36] M. Cacciari, G. P. Salam, and G. Soyez, “FASTJET user manual”, *Eur. Phys. J. C* **72** (2012) 1896, doi:[10.1140/epjc/s10052-012-1896-2](https://doi.org/10.1140/epjc/s10052-012-1896-2), arXiv:[1111.6097](https://arxiv.org/abs/1111.6097).
- [37] CMS Collaboration, “Pileup mitigation at CMS in 13 TeV data”, *JINST* **15** (2020) P09018, doi:[10.1088/1748-0221/15/09/P09018](https://doi.org/10.1088/1748-0221/15/09/P09018), arXiv:[2003.00503](https://arxiv.org/abs/2003.00503).
- [38] CMS Collaboration, “Jet energy scale and resolution in the CMS experiment in pp collisions at 8 TeV”, *JINST* **12** (2017) P02014, doi:[10.1088/1748-0221/12/02/P02014](https://doi.org/10.1088/1748-0221/12/02/P02014), arXiv:[1607.03663](https://arxiv.org/abs/1607.03663).
- [39] CMS Collaboration, “Performance of missing transverse momentum reconstruction in proton-proton collisions at  $\sqrt{s} = 13$  TeV using the CMS detector”, *JINST* **14** (2019) P07004, doi:[10.1088/1748-0221/14/07/P07004](https://doi.org/10.1088/1748-0221/14/07/P07004), arXiv:[1903.06078](https://arxiv.org/abs/1903.06078).
- [40] CMS Collaboration, “Performance of the CMS muon detector and muon reconstruction with proton-proton collisions at  $\sqrt{s} = 13$  TeV”, *JINST* **13** (2018) P06015, doi:[10.1088/1748-0221/13/06/P06015](https://doi.org/10.1088/1748-0221/13/06/P06015), arXiv:[1804.04528](https://arxiv.org/abs/1804.04528).
- [41] CMS Collaboration, “Performance of electron reconstruction and selection with the CMS detector in proton-proton collisions at  $\sqrt{s} = 8$  TeV”, *JINST* **10** (2015) P06005, doi:[10.1088/1748-0221/10/06/P06005](https://doi.org/10.1088/1748-0221/10/06/P06005), arXiv:[1502.02701](https://arxiv.org/abs/1502.02701).
- [42] CMS Collaboration, “Performance of the CMS Level-1 trigger in proton-proton collisions at  $\sqrt{s} = 13$  TeV”, *JINST* **15** (2020) P10017, doi:[10.1088/1748-0221/15/10/P10017](https://doi.org/10.1088/1748-0221/15/10/P10017), arXiv:[2006.10165](https://arxiv.org/abs/2006.10165).
- [43] CMS Collaboration, “The CMS trigger system”, *JINST* **12** (2017) P01020, doi:[10.1088/1748-0221/12/01/P01020](https://doi.org/10.1088/1748-0221/12/01/P01020), arXiv:[1609.02366](https://arxiv.org/abs/1609.02366).
- [44] J. Alwall et al., “The automated computation of tree-level and next-to-leading order differential cross sections, and their matching to parton shower simulations”, *JHEP* **07** (2014) 079, doi:[10.1007/JHEP07\(2014\)079](https://doi.org/10.1007/JHEP07(2014)079), arXiv:[1405.0301](https://arxiv.org/abs/1405.0301).
- [45] J. Alwall et al., “Comparative study of various algorithms for the merging of parton showers and matrix elements in hadronic collisions”, *Eur. Phys. J. C* **53** (2008) 473, doi:[10.1140/epjc/s10052-007-0490-5](https://doi.org/10.1140/epjc/s10052-007-0490-5), arXiv:[0706.2569](https://arxiv.org/abs/0706.2569).

- [46] R. Frederix and S. Frixione, “Merging meets matching in MC@NLO”, *JHEP* **12** (2012) 061, doi:[10.1007/JHEP12\(2012\)061](https://doi.org/10.1007/JHEP12(2012)061), arXiv:[1209.6215](https://arxiv.org/abs/1209.6215).
- [47] P. Nason, “A new method for combining NLO QCD with shower Monte Carlo algorithms”, *JHEP* **11** (2004) 040, doi:[10.1088/1126-6708/2004/11/040](https://doi.org/10.1088/1126-6708/2004/11/040), arXiv:[hep-ph/0409146](https://arxiv.org/abs/hep-ph/0409146).
- [48] S. Frixione, P. Nason, and C. Oleari, “Matching NLO QCD computations with parton shower simulations: the POWHEG method”, *JHEP* **11** (2007) 070, doi:[10.1088/1126-6708/2007/11/070](https://doi.org/10.1088/1126-6708/2007/11/070), arXiv:[0709.2092](https://arxiv.org/abs/0709.2092).
- [49] S. Alioli, P. Nason, C. Oleari, and E. Re, “NLO single-top production matched with shower in POWHEG: s- and t-channel contributions”, *JHEP* **09** (2009) 111, doi:[10.1088/1126-6708/2009/09/111](https://doi.org/10.1088/1126-6708/2009/09/111), arXiv:[0907.4076](https://arxiv.org/abs/0907.4076). [Erratum: doi:[10.1007/JHEP02\(2010\)011](https://doi.org/10.1007/JHEP02(2010)011)].
- [50] S. Alioli, P. Nason, C. Oleari, and E. Re, “A general framework for implementing NLO calculations in shower Monte Carlo programs: the POWHEG BOX”, *JHEP* **06** (2010) 043, doi:[10.1007/JHEP06\(2010\)043](https://doi.org/10.1007/JHEP06(2010)043), arXiv:[1002.2581](https://arxiv.org/abs/1002.2581).
- [51] E. Re, “Single-top Wt-channel production matched with parton showers using the POWHEG method”, *Eur. Phys. J. C* **71** (2011) 1547, doi:[10.1140/epjc/s10052-011-1547-z](https://doi.org/10.1140/epjc/s10052-011-1547-z), arXiv:[1009.2450](https://arxiv.org/abs/1009.2450).
- [52] J. M. Campbell, R. K. Ellis, P. Nason, and E. Re, “Top-pair production and decay at NLO matched with parton showers”, *JHEP* **04** (2015) 114, doi:[10.1007/JHEP04\(2015\)114](https://doi.org/10.1007/JHEP04(2015)114), arXiv:[1412.1828](https://arxiv.org/abs/1412.1828).
- [53] T. Sjöstrand et al., “An introduction to PYTHIA 8.2”, *Comput. Phys. Commun.* **191** (2015) 159, doi:[10.1016/j.cpc.2015.01.024](https://doi.org/10.1016/j.cpc.2015.01.024), arXiv:[1410.3012](https://arxiv.org/abs/1410.3012).
- [54] S. Alioli, P. Nason, C. Oleari, and E. Re, “NLO Higgs boson production via gluon fusion matched with shower in POWHEG”, *JHEP* **04** (2009) 002, doi:[10.1088/1126-6708/2009/04/002](https://doi.org/10.1088/1126-6708/2009/04/002), arXiv:[0812.0578](https://arxiv.org/abs/0812.0578).
- [55] NNPDF Collaboration, “Parton distributions for the LHC Run II”, *JHEP* **04** (2015) 040, doi:[10.1007/JHEP04\(2015\)040](https://doi.org/10.1007/JHEP04(2015)040), arXiv:[1410.8849](https://arxiv.org/abs/1410.8849).
- [56] NNPDF Collaboration, “Parton distributions from high-precision collider data”, *Eur. Phys. J. C* **77** (2017) 663, doi:[10.1140/epjc/s10052-017-5199-5](https://doi.org/10.1140/epjc/s10052-017-5199-5), arXiv:[1706.00428](https://arxiv.org/abs/1706.00428).
- [57] CMS Collaboration, “Extraction and validation of a new set of CMS PYTHIA8 tunes from underlying-event measurements”, *Eur. Phys. J. C* **80** (2020) 4, doi:[10.1140/epjc/s10052-019-7499-4](https://doi.org/10.1140/epjc/s10052-019-7499-4), arXiv:[1903.12179](https://arxiv.org/abs/1903.12179).
- [58] N. Davidson et al., “Universal interface of TAUOLA technical and physics documentation”, *Comput. Phys. Commun.* **183** (2012) 821, doi:[10.1016/j.cpc.2011.12.009](https://doi.org/10.1016/j.cpc.2011.12.009), arXiv:[1002.0543](https://arxiv.org/abs/1002.0543).
- [59] GEANT4 Collaboration, “GEANT4—a simulation toolkit”, *Nucl. Instrum. Meth. A* **506** (2003) 250, doi:[10.1016/S0168-9002\(03\)01368-8](https://doi.org/10.1016/S0168-9002(03)01368-8).
- [60] Particle Data Group, P. A. Zyla et al., “Review of particle physics”, *Prog. Theor. Exp. Phys.* **2020** (2020) 083C01, doi:[10.1093/ptep/ptaa104](https://doi.org/10.1093/ptep/ptaa104).

- [61] D. Bertolini, P. Harris, M. Low, and N. Tran, “Pileup per particle identification”, *JHEP* **10** (2014) 059, doi:10.1007/JHEP10(2014)059, arXiv:1407.6013.
- [62] I. J. Goodfellow, Y. Bengio, and A. Courville, “Deep Learning”. MIT Press, Cambridge, MA, USA, 2016. <http://www.deeplearningbook.org>.
- [63] S. Ioffe and C. Szegedy, “Batch normalization: Accelerating deep network training by reducing internal covariate shift”, 2015. arXiv:1502.03167.
- [64] G. E. Hinton et al., “Improving neural networks by preventing co-adaptation of feature detectors”, 2012. arXiv:1207.0580.
- [65] N. Srivastava et al., “Dropout: A simple way to prevent neural networks from overfitting”, *J. Mach. Learn. Res.* **15** (2014) 1929.
- [66] K. He, X. Zhang, S. Ren, and J. Sun, “Delving deep into rectifiers: Surpassing human-level performance on ImageNet classification”, 2015. arXiv:1502.01852.
- [67] T.-Y. Lin et al., “Focal loss for dense object detection”, *TPAMI* **42** (2018) 318, doi:10.1109/TPAMI.2018.2858826, arXiv:1708.02002.
- [68] T. Dozat, “Incorporating Nesterov momentum into ADAM”, in *Conference Track Proceedings, 4th International Conference on Learning Representations (ICLR 2016)*. 2016.
- [69] D. P. Kingma and J. Ba, “Adam: A method for stochastic optimization”, in *Conference Track Proceedings, 3rd International Conference on Learning Representations (ICLR 2015)*. 2015. arXiv:1412.6980.
- [70] F. Chollet et al., “Keras”. <https://keras.io>, 2015.
- [71] M. Abadi et al., “TensorFlow: Large-scale machine learning on heterogeneous systems”, 2015. Software available from tensorflow.org. <https://www.tensorflow.org/>.
- [72] CMS Collaboration, “Measurements of Higgs boson production in the decay channel with a pair of  $\tau$  leptons in proton-proton collisions at  $\sqrt{s} = 13$  TeV”, 2022. arXiv:2204.12957. Submitted to *Eur. Phys. J. C*.
- [73] CMS Collaboration, “Measurement of the Higgs boson production rate in association with top quarks in final states with electrons, muons, and hadronically decaying tau leptons at  $\sqrt{s} = 13$  TeV”, *Eur. Phys. J. C* **81** (2021) 378, doi:10.1140/epjc/s10052-021-09014-x, arXiv:2011.03652.
- [74] CMS Collaboration, “Search for singly and pair-produced leptoquarks coupling to third-generation fermions in proton-proton collisions at  $\sqrt{s} = 13$  TeV”, *Phys. Lett. B* **819** (2021) 136446, doi:10.1016/j.physletb.2021.136446, arXiv:2012.04178.
- [75] CMS Collaboration, “Precision luminosity measurement in proton-proton collisions at  $\sqrt{s} = 13$  TeV in 2015 and 2016 at CMS”, *Eur. Phys. J. C* **81** (2021) 800, doi:10.1140/epjc/s10052-021-09538-2, arXiv:2104.01927.
- [76] CMS Collaboration, “CMS luminosity measurement for the 2017 data-taking period at  $\sqrt{s} = 13$  TeV”, CMS Physics Analysis Summary CMS-PAS-LUM-17-004, 2018.
- [77] CMS Collaboration, “CMS luminosity measurement for the 2018 data-taking period at  $\sqrt{s} = 13$  TeV”, CMS Physics Analysis Summary CMS-PAS-LUM-18-002, 2019.

- [78] G. Cowan, K. Cranmer, E. Gross, and O. Vitells, “Asymptotic formulae for likelihood-based tests of new physics”, *Eur. Phys. J. C* **71** (2011) 1554, doi:[10.1140/epjc/s10052-011-1554-0](https://doi.org/10.1140/epjc/s10052-011-1554-0), arXiv:[1007.1727](https://arxiv.org/abs/1007.1727). [Erratum: doi:[10.1140/epjc/s10052-013-2501-z](https://doi.org/10.1140/epjc/s10052-013-2501-z)].
- [79] CMS Collaboration, “Measurements of inclusive W and Z cross sections in pp collisions at  $\sqrt{s} = 7$  TeV”, *JHEP* **01** (2011) 080, doi:[10.1007/JHEP01\(2011\)080](https://doi.org/10.1007/JHEP01(2011)080), arXiv:[1012.2466](https://arxiv.org/abs/1012.2466).

## A Loss function

The loss function used for the training of the DEEPTAU algorithm has the form

$$\begin{aligned}
L(\mathbf{y}^{\text{true}}, \mathbf{y}; \boldsymbol{\kappa}, \boldsymbol{\gamma}, \boldsymbol{\omega}) = & \underbrace{\kappa_\tau H_\tau(\mathbf{y}^{\text{true}}, \mathbf{y}; \boldsymbol{\omega})}_{\text{(a) Separation of all } \alpha} + \underbrace{\left( \kappa_e + \kappa_\mu + \kappa_{\text{jet}} \right) \bar{F}_{\text{cmb}}(1 - y_\tau^{\text{true}}, 1 - y_\tau; \gamma_{\text{cmb}})}_{\text{(b) Focused separation of}} \\
& \quad e, \mu, \text{jet from } \tau_h \\
& + \underbrace{\kappa_F \sum_{i \in \{e, \mu, \text{jet}\}} \kappa_i \hat{\theta}(y_\tau - 0.1) \bar{F}_i(y_i^{\text{true}}, y_i; \gamma_i)}_{\text{(c) Focused separation of } \tau_h \text{ from } e, \mu, \text{jet for } y_\tau > 0.1}.
\end{aligned} \tag{A.1}$$

**Categorical cross entropy:**

$$H(\mathbf{y}^{\text{true}}, \mathbf{y}; \boldsymbol{\omega}) = - \sum_{\alpha} \omega_{\alpha} y_{\alpha}^{\text{true}} y_{\alpha}; \quad \alpha \in \{\tau, e, \mu, \text{jet}\}.$$

**Focal loss function:**

$$F(y^{\text{true}}, y; \gamma) = -y^{\text{true}} (1 - y)^{\gamma} \log(y) \quad \bar{F}(y^{\text{true}}, y; \gamma) = \mathcal{N} F(y^{\text{true}}, y; \gamma),$$

where bold fonts indicate groups of parameters;  $H(\cdot, \cdot; \cdot)$  corresponds to the categorical cross entropy and  $F(\cdot, \cdot; \cdot)$  to the focal loss function [67];  $\mathcal{N}$  is a factor to normalize  $F(\cdot, \cdot; \cdot)$  to unity in the interval 0–1; and  $\hat{\theta}(\cdot)$  is a smoothed step function that approaches 1 for  $y_\tau > 0.1$ . The focal loss terms in Eq. A.1(b) and (c) put more emphasis on the part of parameter space in which it is more difficult to separate  $\tau_h$  candidates from  $e$ ,  $\mu$ , and jets. The step function in Eq. A.1(c) disregards the part of parameter space in which the probability for the  $\tau_h$  candidate to correspond to a genuine  $\tau_h$  is low, for which we are not interested in optimal separation between  $e$ ,  $\mu$ , and jets.

The values and meanings of the parameters  $\boldsymbol{\kappa}$ ,  $\boldsymbol{\gamma}$ , and  $\boldsymbol{\omega}$  are given in Table A.1. The values of the  $\kappa$ -factors are chosen such that the numerical values of the different components of the loss function are close to each other, while putting more emphasis on the discrimination against jets, since jets are the dominant source of background.

Table A.1: Parameters used in the definition of the loss function for the training of the DEEPTAU algorithm.

Parameter	Value	Location in Eq. A.1			Meaning
		(a)	(b)	(c)	
$\kappa_\tau$	2.0	✓			$\tau_h$
$\kappa_e$	0.4	✓	✓	✓	Emphasis on e separation
$\kappa_\mu$	1.0	✓	✓	✓	$\mu$ separation
$\kappa_{jet}$	0.6	✓	✓	✓	jet
$\kappa_F$	5.0			✓	Emphasis on high $\tau_h$ efficiency
$\gamma_e$	2.0			✓	e
$\gamma_\mu$	2.0			✓	Focus on $\mu$ separation
$\gamma_{jet}$	0.5			✓	jet
$\gamma_{cmb}$	2.0		✓		e, $\mu$ , jet
$\omega_\alpha$	varying	✓			Sample normalization

## B The CMS Collaboration

**Yerevan Physics Institute, Yerevan, Armenia**

A. Tumasyan

**Institut für Hochenergiephysik, Vienna, Austria**

W. Adam , J.W. Andrejkovic, T. Bergauer , S. Chatterjee , M. Dragicevic , A. Escalante Del Valle , R. Frühwirth<sup>1</sup>, M. Jeitler<sup>1</sup> , N. Krammer, L. Lechner , D. Liko, I. Mikulec, P. Paulitsch, F.M. Pitters, J. Schieck<sup>1</sup> , R. Schöfbeck , D. Schwarz, S. Templ , W. Waltenberger , C.-E. Wulz<sup>1</sup> 

**Institute for Nuclear Problems, Minsk, Belarus**

V. Chekhovsky, A. Litomin, V. Makarenko 

**Universiteit Antwerpen, Antwerpen, Belgium**

M.R. Darwish<sup>2</sup>, E.A. De Wolf, T. Janssen , T. Kello<sup>3</sup>, A. Lelek , H. Rejeb Sfar, P. Van Mechelen , S. Van Putte, N. Van Remortel 

**Vrije Universiteit Brussel, Brussel, Belgium**

F. Blekman , E.S. Bols , J. D'Hondt , M. Delcourt, H. El Faham , S. Lowette , S. Moortgat , A. Morton , D. Müller , A.R. Sahasransu , S. Tavernier , W. Van Doninck, P. Van Mulders

**Université Libre de Bruxelles, Bruxelles, Belgium**

D. Beghin, B. Bilin , B. Clerbaux , G. De Lentdecker, L. Favart , A. Grebenyuk, A.K. Kalsi , K. Lee, M. Mahdavikhorrami, I. Makarenko , L. Moureaux , L. Pétré, A. Popov , N. Postiau, E. Starling , L. Thomas , M. Vanden Bemden, C. Vander Velde , P. Vanlaer , L. Wezenbeek

**Ghent University, Ghent, Belgium**

T. Cornelis , D. Dobur, J. Knolle , L. Lambrecht, G. Mestdach, M. Niedziela , C. Roskas, A. Samalan, K. Skovpen , M. Tytgat , B. Vermassen, M. Vit

**Université Catholique de Louvain, Louvain-la-Neuve, Belgium**

A. Benecke, A. Bethani , G. Bruno, F. Bury , C. Caputo , P. David , C. Delaere , I.S. Donertas , A. Giannanco , K. Jaffel, Sa. Jain , V. Lemaitre, K. Mondal , J. Prisciandaro, A. Taliercio, M. Teklishyn , T.T. Tran, P. Vischia , S. Wertz 

**Centro Brasileiro de Pesquisas Fisicas, Rio de Janeiro, Brazil**

G.A. Alves , C. Hensel, A. Moraes 

**Universidade do Estado do Rio de Janeiro, Rio de Janeiro, Brazil**

W.L. Aldá Júnior , M. Alves Gallo Pereira , M. Barroso Ferreira Filho, H. Brandao Malbouisson, W. Carvalho , J. Chinellato<sup>4</sup>, E.M. Da Costa , G.G. Da Silveira<sup>5</sup> , D. De Jesus Damiao , S. Fonseca De Souza , D. Matos Figueiredo, C. Mora Herrera , K. Mota Amarilo, L. Mundim , H. Nogima, P. Rebello Teles , A. Santoro, S.M. Silva Do Amaral , A. Sznajder , M. Thiel, F. Torres Da Silva De Araujo<sup>6</sup> , A. Vilela Pereira 

**Universidade Estadual Paulista (a), Universidade Federal do ABC (b), São Paulo, Brazil**

C.A. Bernardes<sup>5</sup> , L. Calligaris , T.R. Fernandez Perez Tomei , E.M. Gregores , D.S. Lemos , P.G. Mercadante , S.F. Novaes , Sandra S. Padula 

**Institute for Nuclear Research and Nuclear Energy, Bulgarian Academy of Sciences, Sofia, Bulgaria**

A. Aleksandrov, G. Antchev , R. Hadjiiska, P. Iaydjiev, M. Misheva, M. Rodozov, M. Shopova,

G. Sultanov

**University of Sofia, Sofia, Bulgaria**

A. Dimitrov, T. Ivanov, L. Litov , B. Pavlov, P. Petkov, A. Petrov

**Beihang University, Beijing, China**

T. Cheng , T. Javaid<sup>7</sup>, M. Mittal, L. Yuan

**Department of Physics, Tsinghua University, Beijing, China**

M. Ahmad , G. Bauer, C. Dozen<sup>8</sup> , Z. Hu , J. Martins<sup>9</sup> , Y. Wang, K. Yi<sup>10,11</sup>

**Institute of High Energy Physics, Beijing, China**

E. Chapon , G.M. Chen<sup>7</sup> , H.S. Chen<sup>7</sup> , M. Chen , F. Iemmi, A. Kapoor , D. Leggat, H. Liao, Z.-A. Liu<sup>7</sup> , V. Milosevic , F. Monti , R. Sharma , J. Tao , J. Thomas-Wilsker, J. Wang , H. Zhang , J. Zhao 

**State Key Laboratory of Nuclear Physics and Technology, Peking University, Beijing, China**

A. Agapitos, Y. An, Y. Ban, C. Chen, A. Levin , Q. Li , X. Lyu, Y. Mao, S.J. Qian, D. Wang , Q. Wang , J. Xiao

**Sun Yat-Sen University, Guangzhou, China**

M. Lu, Z. You 

**Institute of Modern Physics and Key Laboratory of Nuclear Physics and Ion-beam Application (MOE) - Fudan University, Shanghai, China**

X. Gao<sup>3</sup>, H. Okawa 

**Zhejiang University, Hangzhou, China, Zhejiang, China**

Z. Lin , M. Xiao 

**Universidad de Los Andes, Bogota, Colombia**

C. Avila , A. Cabrera , C. Florez , J. Fraga

**Universidad de Antioquia, Medellin, Colombia**

J. Mejia Guisao, F. Ramirez, J.D. Ruiz Alvarez , C.A. Salazar Gonzalez 

**University of Split, Faculty of Electrical Engineering, Mechanical Engineering and Naval Architecture, Split, Croatia**

D. Giljanovic, N. Godinovic , D. Lelas , I. Puljak 

**University of Split, Faculty of Science, Split, Croatia**

Z. Antunovic, M. Kovac, T. Sculac 

**Institute Rudjer Boskovic, Zagreb, Croatia**

V. Brigljevic , D. Ferencek , D. Majumder , M. Roguljic, A. Starodumov<sup>12</sup> , T. Susa 

**University of Cyprus, Nicosia, Cyprus**

A. Attikis , K. Christoforou, E. Erodotou, A. Ioannou, G. Kole , M. Kolosova, S. Konstantinou, J. Mousa , C. Nicolaou, F. Ptochos , P.A. Razis, H. Rykaczewski, H. Saka 

**Charles University, Prague, Czech Republic**

M. Finger<sup>13</sup>, M. Finger Jr.<sup>13</sup> , A. Kveton

**Escuela Politecnica Nacional, Quito, Ecuador**

E. Ayala

**Universidad San Francisco de Quito, Quito, Ecuador**

E. Carrera Jarrin 

**Academy of Scientific Research and Technology of the Arab Republic of Egypt, Egyptian Network of High Energy Physics, Cairo, Egypt**

A. Ellithi Kamel<sup>14</sup>, E. Salama<sup>15,16</sup>

**Center for High Energy Physics (CHEP-FU), Fayoum University, El-Fayoum, Egypt**

A. Lotfy , M.A. Mahmoud 

**National Institute of Chemical Physics and Biophysics, Tallinn, Estonia**

S. Bhowmik , R.K. Dewanjee , K. Ehataht, M. Kadastik, S. Nandan, C. Nielsen, J. Pata, M. Raidal , L. Tani, C. Veelken

**Department of Physics, University of Helsinki, Helsinki, Finland**

P. Eerola , L. Forthomme , H. Kirschenmann , K. Osterberg , M. Voutilainen 

**Helsinki Institute of Physics, Helsinki, Finland**

S. Bharthuar, E. Brückner , F. Garcia , J. Havukainen , M.S. Kim , R. Kinnunen, T. Lampén, K. Lassila-Perini , S. Lehti , T. Lindén, M. Lotti, L. Martikainen, M. Myllymäki, J. Ott , H. Siikonen, E. Tuominen , J. Tuomiemi

**Lappeenranta University of Technology, Lappeenranta, Finland**

P. Luukka , H. Petrow, T. Tuuva

**IRFU, CEA, Université Paris-Saclay, Gif-sur-Yvette, France**

C. Amendola , M. Besancon, F. Couderc , M. Dejardin, D. Denegri, J.L. Faure, F. Ferri , S. Ganjour, A. Givernaud, P. Gras, G. Hamel de Monchenault , P. Jarry, B. Lenzi , E. Locci, J. Malcles, J. Rander, A. Rosowsky , M.Ö. Sahin , A. Savoy-Navarro<sup>17</sup>, M. Titov , G.B. Yu 

**Laboratoire Leprince-Ringuet, CNRS/IN2P3, Ecole Polytechnique, Institut Polytechnique de Paris, Palaiseau, France**

S. Ahuja , F. Beaudette , M. Bonanomi , A. Buchot Perraguin, P. Busson, A. Cappati, C. Charlot, O. Davignon, B. Diab, G. Falmagne , S. Ghosh, R. Granier de Cassagnac , A. Hakimi, I. Kucher , J. Motta, M. Nguyen , C. Ochando , P. Paganini , J. Rembser, R. Salerno , U. Sarkar , J.B. Sauvan , Y. Sirois , A. Tarabini, A. Zabi, A. Zghiche 

**Université de Strasbourg, CNRS, IPHC UMR 7178, Strasbourg, France**

J.-L. Agram<sup>18</sup> , J. Andrea, D. Apparu, D. Bloch , G. Bourgatte, J.-M. Brom, E.C. Chabert, C. Collard , D. Darej, J.-C. Fontaine<sup>18</sup>, U. Goerlach, C. Grimault, A.-C. Le Bihan, E. Nibigira , P. Van Hove 

**Institut de Physique des 2 Infinis de Lyon (IP2I ), Villeurbanne, France**

E. Asilar , S. Beauceron , C. Bernet , G. Boudoul, C. Camen, A. Carle, N. Chanon , D. Contardo, P. Depasse , H. El Mamouni, J. Fay, S. Gascon , M. Gouzevitch , B. Ille, I.B. Laktineh, H. Lattaud , A. Lesauvage , M. Lethuillier , L. Mirabito, S. Perries, K. Shchablo, V. Sordini , L. Torterotot , G. Touquet, M. Vander Donckt, S. Viret

**Georgian Technical University, Tbilisi, Georgia**

G. Adamov, I. Lomidze, Z. Tsamalaidze<sup>13</sup>

**RWTH Aachen University, I. Physikalisches Institut, Aachen, Germany**

V. Botta, L. Feld , K. Klein, M. Lipinski, D. Meuser, A. Pauls, N. Röwert, J. Schulz, M. Teroerde 

**RWTH Aachen University, III. Physikalisches Institut A, Aachen, Germany**

A. Dodonova, D. Eliseev, M. Erdmann , P. Fackeldey , B. Fischer, S. Ghosh , T. Hebbeker , K. Hoepfner, F. Ivone, L. Mastrolorenzo, M. Merschmeyer , A. Meyer 

G. Mocellin, S. Mondal, S. Mukherjee , D. Noll , A. Novak, T. Pook , A. Pozdnyakov , Y. Rath, H. Reithler, J. Roemer, A. Schmidt , S.C. Schuler, A. Sharma , L. Vigilante, S. Wiedenbeck, S. Zaleski

**RWTH Aachen University, III. Physikalisches Institut B, Aachen, Germany**

C. Dziwok, G. Flügge, W. Haj Ahmad<sup>19</sup> , O. Hlushchenko, T. Kress, A. Nowack , C. Pistone, O. Pooth, D. Roy , H. Sert , A. Stahl<sup>20</sup> , T. Ziemons , A. Zotz

**Deutsches Elektronen-Synchrotron, Hamburg, Germany**

H. Aarup Petersen, M. Aldaya Martin, P. Asmuss, S. Baxter, M. Bayatmakou, O. Behnke, A. Bermúdez Martínez, S. Bhattacharya, A.A. Bin Anuar , K. Borras<sup>21</sup>, D. Brunner, A. Campbell , A. Cardini , C. Cheng, F. Colombina, S. Consuegra Rodríguez , G. Correia Silva, V. Danilov, M. De Silva, L. Didukh, G. Eckerlin, D. Eckstein, L.I. Estevez Banos , O. Filatov , E. Gallo<sup>22</sup>, A. Geiser, A. Giraldi, A. Grohsjean , M. Guthoff, A. Jafari<sup>23</sup> , N.Z. Jomhari , H. Jung , A. Kasem<sup>21</sup> , M. Kasemann , H. Kaveh , C. Kleinwort , D. Krücker , W. Lange, T. Lenz, J. Lidrych , K. Lipka, W. Lohmann<sup>24</sup>, R. Mankel, I.-A. Melzer-Pellmann , M. Mendizabal Morentin, J. Metwally, A.B. Meyer , M. Meyer , J. Mnich , A. Mussgiller, Y. Otarid, D. Pérez Adán , D. Pitzl, A. Raspereza, B. Ribeiro Lopes, J. Rübenach, A. Saggio , A. Saibel , M. Savitskyi , M. Scham<sup>25</sup>, V. Scheurer, P. Schütze, C. Schwanenberger<sup>22</sup> , A. Singh, R.E. Sosa Ricardo , D. Stafford, N. Tonon , M. Van De Klundert , R. Walsh , D. Walter, Y. Wen , K. Wichmann, L. Wiens, C. Wissing, S. Wuchterl 

**University of Hamburg, Hamburg, Germany**

R. Aggleton, S. Albrecht , S. Bein , L. Benato , P. Connor , K. De Leo , M. Eich, F. Feindt, A. Fröhlich, C. Garbers , E. Garutti , P. Gunnellini, M. Hajheidari, J. Haller , A. Hinzmann , G. Kasieczka, R. Klanner , R. Kogler , T. Kramer, V. Kutzner, J. Lange , T. Lange , A. Lobanov , A. Malara , A. Nigamova, K.J. Pena Rodriguez, O. Rieger, P. Schleper, M. Schröder , J. Schwandt , J. Sonneveld , H. Stadie, G. Steinbrück, A. Tews, I. Zoi 

**Karlsruher Institut fuer Technologie, Karlsruhe, Germany**

J. Bechtel , S. Brommer, M. Burkart, E. Butz , R. Caspart , T. Chwalek, W. De Boer<sup>†</sup>, A. Dierlamm, A. Droll, K. El Morabit, N. Faltermann , M. Giffels, J.o. Gosewisch, A. Gottmann, F. Hartmann<sup>20</sup> , C. Heidecker, U. Husemann , P. Keicher, R. Koppenhöfer, S. Maier, M. Metzler, S. Mitra , Th. Müller, M. Neukum, A. Nürnberg, G. Quast , K. Rabbertz , J. Rauser, D. Savoiu , M. Schnepf, D. Seith, I. Shvetsov, H.J. Simonis, R. Ulrich , J. Van Der Linden, R.F. Von Cube, M. Wassmer, M. Weber , S. Wieland, R. Wolf , S. Wozniewski, S. Wunsch

**Institute of Nuclear and Particle Physics (INPP), NCSR Demokritos, Aghia Paraskevi, Greece**

G. Anagnostou, G. Daskalakis, T. Geralis , A. Kyriakis, D. Loukas, A. Stakia 

**National and Kapodistrian University of Athens, Athens, Greece**

M. Diamantopoulou, D. Karasavvas, G. Karathanasis, P. Kontaxakis , C.K. Koraka, A. Manousakis-Katsikakis, A. Panagiotou, I. Papavergou, N. Saoulidou , K. Theofilatos , E. Tziaferi , K. Vellidis, E. Vourliotis

**National Technical University of Athens, Athens, Greece**

G. Bakas, K. Kousouris , I. Papakrivopoulos, G. Tsipolitis, A. Zacharopoulou

**University of Ioánnina, Ioánnina, Greece**

K. Adamidis, I. Bestintzanos, I. Evangelou , C. Foudas, P. Gianneios, P. Katsoulis, P. Kokkas,

N. Manthos, I. Papadopoulos , J. Strologas 

**MTA-ELTE Lendület CMS Particle and Nuclear Physics Group, Eötvös Loránd University, Budapest, Hungary**

M. Csanad , K. Farkas, M.M.A. Gadallah<sup>26</sup> , S. Lököс<sup>27</sup> , P. Major, K. Mandal , A. Mehta , G. Pasztor , A.J. Rádl, O. Surányi, G.I. Veres 

**Wigner Research Centre for Physics, Budapest, Hungary**

M. Bartók<sup>28</sup> , G. Bencze, C. Hajdu , D. Horvath<sup>29</sup> , F. Sikler , V. Veszpremi 

**Institute of Nuclear Research ATOMKI, Debrecen, Hungary**

S. Czellar, J. Karancsi<sup>28</sup> , J. Molnar, Z. Szillasi, D. Teyssier

**Institute of Physics, University of Debrecen, Debrecen, Hungary**

P. Raics, Z.L. Trocsanyi<sup>30</sup> , B. Ujvari

**Karoly Robert Campus, MATE Institute of Technology, Gyongyos, Hungary**

T. Csorgo<sup>31</sup> , F. Nemes<sup>31</sup>, T. Novak

**Indian Institute of Science (IISc), Bangalore, India**

S. Choudhury, J.R. Komaragiri , D. Kumar, L. Panwar , P.C. Tiwari 

**National Institute of Science Education and Research, HBNI, Bhubaneswar, India**

S. Bahinipati<sup>32</sup> , C. Kar , P. Mal, T. Mishra , V.K. Muraleedharan Nair Bindhu<sup>33</sup>, A. Nayak<sup>33</sup> , P. Saha, N. Sur , S.K. Swain, D. Vats<sup>33</sup>

**Panjab University, Chandigarh, India**

S. Bansal , S.B. Beri, V. Bhatnagar , G. Chaudhary , S. Chauhan , N. Dhingra<sup>34</sup> , R. Gupta, A. Kaur, M. Kaur , S. Kaur, P. Kumari , M. Meena, K. Sandeep , J.B. Singh , A.K. Virdi 

**University of Delhi, Delhi, India**

A. Ahmed, A. Bhardwaj , B.C. Choudhary , M. Gola, S. Keshri , A. Kumar , M. Naimuddin , P. Priyanka , K. Ranjan, A. Shah 

**Saha Institute of Nuclear Physics, HBNI, Kolkata, India**

M. Bharti<sup>35</sup>, R. Bhattacharya, S. Bhattacharya , D. Bhowmik, S. Dutta, S. Dutta, B. Gomber<sup>36</sup> , M. Maity<sup>37</sup>, P. Palit , P.K. Rout , G. Saha, B. Sahu , S. Sarkar, M. Sharan, B. Singh<sup>35</sup>, S. Thakur<sup>35</sup>

**Indian Institute of Technology Madras, Madras, India**

P.K. Behera , S.C. Behera, P. Kalbhor , A. Muhammad, R. Pradhan, P.R. Pujahari, A. Sharma , A.K. Sikdar

**Bhabha Atomic Research Centre, Mumbai, India**

D. Dutta , V. Jha, V. Kumar , D.K. Mishra, K. Naskar<sup>38</sup>, P.K. Netrakanti, L.M. Pant, P. Shukla 

**Tata Institute of Fundamental Research-A, Mumbai, India**

T. Aziz, S. Dugad, M. Kumar

**Tata Institute of Fundamental Research-B, Mumbai, India**

S. Banerjee , R. Chudasama, M. Guchait, S. Karmakar, S. Kumar, G. Majumder, K. Mazumdar, S. Mukherjee 

**Indian Institute of Science Education and Research (IISER), Pune, India**

K. Alpana, S. Dube , B. Kansal, A. Laha, S. Pandey , A. Rane , A. Rastogi , S. Sharma 

**Isfahan University of Technology, Isfahan, Iran**H. Bakhshiansohi<sup>39</sup> , E. Khazaie, M. Zeinali<sup>40</sup>**Institute for Research in Fundamental Sciences (IPM), Tehran, Iran**S. Chenarani<sup>41</sup>, S.M. Etesami , M. Khakzad , M. Mohammadi Najafabadi **University College Dublin, Dublin, Ireland**M. Grunewald **INFN Sezione di Bari <sup>a</sup>, Bari, Italy, Università di Bari <sup>b</sup>, Bari, Italy, Politecnico di Bari <sup>c</sup>, Bari, Italy**

M. Abbrescia<sup>a,b</sup> , R. Aly<sup>a,b,42</sup> , C. Aruta<sup>a,b</sup>, A. Colaleo<sup>a</sup> , D. Creanza<sup>a,c</sup> , N. De Filippis<sup>a,c</sup> , M. De Palma<sup>a,b</sup> , A. Di Florio<sup>a,b</sup>, A. Di Pilato<sup>a,b</sup> , W. Elmetenawee<sup>a,b</sup> , L. Fiore<sup>a</sup> , A. Gelmi<sup>a,b</sup> , M. Gul<sup>a</sup> , G. Iaselli<sup>a,c</sup> , M. Ince<sup>a,b</sup> , S. Lezki<sup>a,b</sup> , G. Maggi<sup>a,c</sup> , M. Maggi<sup>a</sup> , I. Margjeka<sup>a,b</sup>, V. Mastrapasqua<sup>a,b</sup> , J.A. Merlin<sup>a</sup>, S. My<sup>a,b</sup> , S. Nuzzo<sup>a,b</sup> , A. Pellecchia<sup>a,b</sup>, A. Pompili<sup>a,b</sup> , G. Pugliese<sup>a,c</sup> , D. Ramos, A. Ranieri<sup>a</sup> , G. Selvaggi<sup>a,b</sup> , L. Silvestris<sup>a</sup> , F.M. Simone<sup>a,b</sup> , R. Venditti<sup>a</sup> , P. Verwilligen<sup>a</sup> 

**INFN Sezione di Bologna <sup>a</sup>, Bologna, Italy, Università di Bologna <sup>b</sup>, Bologna, Italy**

G. Abbiendi<sup>a</sup> , C. Battilana<sup>a,b</sup> , D. Bonacorsi<sup>a,b</sup> , L. Borgonovi<sup>a</sup>, L. Brigliadori<sup>a</sup>, R. Campanini<sup>a,b</sup> , P. Capiluppi<sup>a,b</sup> , A. Castro<sup>a,b</sup> , F.R. Cavallo<sup>a</sup> , M. Cuffiani<sup>a,b</sup> , G.M. Dallavalle<sup>a</sup> , T. Diotalevi<sup>a,b</sup> , F. Fabbri<sup>a</sup> , A. Fanfani<sup>a,b</sup> , P. Giacomelli<sup>a</sup> , L. Giommia<sup>a,b</sup> , C. Grandi<sup>a</sup> , L. Guiducci<sup>a,b</sup>, S. Lo Meo<sup>a,43</sup> , L. Lunerti<sup>a,b</sup>, S. Marcellini<sup>a</sup> , G. Masetti<sup>a</sup> , F.L. Navarreria<sup>a,b</sup> , A. Perrotta<sup>a</sup> , F. Primavera<sup>a,b</sup> , A.M. Rossi<sup>a,b</sup> , T. Rovelli<sup>a,b</sup> , G.P. Siroli<sup>a,b</sup> 

**INFN Sezione di Catania <sup>a</sup>, Catania, Italy, Università di Catania <sup>b</sup>, Catania, Italy**

S. Albergo<sup>a,b,44</sup> , S. Costa<sup>a,b,44</sup> , A. Di Mattia<sup>a</sup> , R. Potenza<sup>a,b</sup>, A. Tricomi<sup>a,b,44</sup> , C. Tuve<sup>a,b</sup> 

**INFN Sezione di Firenze <sup>a</sup>, Firenze, Italy, Università di Firenze <sup>b</sup>, Firenze, Italy**

G. Barbagli<sup>a</sup> , A. Cassese<sup>a</sup> , R. Ceccarelli<sup>a,b</sup> , V. Ciulli<sup>a,b</sup> , C. Civinini<sup>a</sup> , R. D'Alessandro<sup>a,b</sup> , E. Focardia<sup>a,b</sup> , G. Latino<sup>a,b</sup> , P. Lenzi<sup>a,b</sup> , M. Lizzo<sup>a,b</sup>, M. Meschini<sup>a</sup> , S. Paoletti<sup>a</sup> , R. Seidita<sup>a,b</sup>, G. Sguazzoni<sup>a</sup> , L. Viliani<sup>a</sup> 

**INFN Laboratori Nazionali di Frascati, Frascati, Italy**L. Benussi , S. Bianco , D. Piccolo **INFN Sezione di Genova <sup>a</sup>, Genova, Italy, Università di Genova <sup>b</sup>, Genova, Italy**M. Bozzo<sup>a,b</sup> , F. Ferro<sup>a</sup> , R. Mulargia<sup>a,b</sup>, E. Robutti<sup>a</sup> , S. Tosi<sup>a,b</sup> **INFN Sezione di Milano-Bicocca <sup>a</sup>, Milano, Italy, Università di Milano-Bicocca <sup>b</sup>, Milano, Italy**

A. Benaglia<sup>a</sup> , G. Boldrini , F. Brivio<sup>a,b</sup> , F. Cetorelli<sup>a,b</sup> , F. De Guio<sup>a,b</sup> , M.E. Dinardo<sup>a,b</sup> , P. Dini<sup>a</sup> , S. Gennai<sup>a</sup> , A. Ghezzi<sup>a,b</sup> , P. Govoni<sup>a,b</sup> , L. Guzzi<sup>a,b</sup> , M.T. Lucchini<sup>a,b</sup> , M. Malberti<sup>a</sup>, S. Malvezzi<sup>a</sup> , A. Massironi<sup>a</sup> , D. Menasce<sup>a</sup> , L. Moroni<sup>a</sup> , M. Paganoni<sup>a,b</sup> , D. Pedrini<sup>a</sup> , B.S. Pinolini, S. Ragazzi<sup>a,b</sup> , N. Redaelli<sup>a</sup> , T. Tabarelli de Fatis<sup>a,b</sup> , D. Valsecchi<sup>a,b,20</sup> , D. Zuolo<sup>a,b</sup> 

**INFN Sezione di Napoli <sup>a</sup>, Napoli, Italy, Università di Napoli 'Federico II' <sup>b</sup>, Napoli, Italy, Università della Basilicata <sup>c</sup>, Potenza, Italy, Università G. Marconi <sup>d</sup>, Roma, Italy**

S. Buontempo<sup>a</sup> , F. Carnevali<sup>a,b</sup> , N. Cavallo<sup>a,c</sup> , A. De Iorio<sup>a,b</sup> , F. Fabozzi<sup>a,c</sup> , A.O.M. Iorio<sup>a,b</sup> , L. Lista<sup>a,b</sup> , S. Meola<sup>a,d,20</sup> , P. Paolucci<sup>a,20</sup> , B. Rossi<sup>a</sup> , C. Sciacca<sup>a,b</sup> 

**INFN Sezione di Padova <sup>a</sup>, Padova, Italy, Università di Padova <sup>b</sup>, Padova, Italy, Università**

**di Trento <sup>c</sup>, Trento, Italy**

P. Azzi<sup>a</sup> , N. Bacchetta<sup>a</sup> , D. Bisello<sup>a,b</sup> , P. Bortignon<sup>a</sup> , A. Bragagnolo<sup>a,b</sup> , R. Carlin<sup>a,b</sup> , P. Checchia<sup>a</sup> , T. Dorigo<sup>a</sup> , U. Dosselli<sup>a</sup> , F. Gasparini<sup>a,b</sup> , U. Gasparini<sup>a,b</sup> , G. Grossi, S.Y. Hoh<sup>a,b</sup> , L. Layer<sup>a,45</sup>, E. Lusiani , M. Margoni<sup>a,b</sup> , A.T. Meneguzzo<sup>a,b</sup> , J. Pazzini<sup>a,b</sup> , M. Presilla<sup>a,b</sup> , P. Ronchese<sup>a,b</sup> , R. Rossin<sup>a,b</sup>, F. Simonetto<sup>a,b</sup> , G. Strong<sup>a</sup> , M. Tosi<sup>a,b</sup> , H. Yarar<sup>a,b</sup>, M. Zanetti<sup>a,b</sup> , P. Zotto<sup>a,b</sup> , A. Zucchetta<sup>a,b</sup> , G. Zumerle<sup>a,b</sup> 

**INFN Sezione di Pavia <sup>a</sup>, Pavia, Italy, Università di Pavia <sup>b</sup>, Pavia, Italy**

C. Aime<sup>a,b</sup>, A. Braghieri<sup>a</sup> , S. Calzaferri<sup>a,b</sup>, D. Fiorina<sup>a,b</sup> , P. Montagna<sup>a,b</sup>, S.P. Ratti<sup>a,b</sup>, V. Re<sup>a</sup> , C. Riccardi<sup>a,b</sup> , P. Salvini<sup>a</sup> , I. Vai<sup>a</sup> , P. Vitulo<sup>a,b</sup> 

**INFN Sezione di Perugia <sup>a</sup>, Perugia, Italy, Università di Perugia <sup>b</sup>, Perugia, Italy**

P. Asenov<sup>a,46</sup> , G.M. Bilei<sup>a</sup> , D. Ciangottini<sup>a,b</sup> , L. Fanò<sup>a,b</sup> , P. Lariccia<sup>a,b</sup>, M. Magherini<sup>b</sup>, G. Mantovani<sup>a,b</sup>, V. Mariani<sup>a,b</sup>, M. Menichelli<sup>a</sup> , F. Moscatelli<sup>a,46</sup> , A. Piccinelli<sup>a,b</sup> , A. Rossi<sup>a,b</sup> , A. Santocchia<sup>a,b</sup> , D. Spiga<sup>a</sup> , T. Tedeschi<sup>a,b</sup> 

**INFN Sezione di Pisa <sup>a</sup>, Pisa, Italy, Università di Pisa <sup>b</sup>, Pisa, Italy, Scuola Normale Superiore di Pisa <sup>c</sup>, Pisa, Italy, Università di Siena <sup>d</sup>, Siena, Italy**

P. Azzurri<sup>a</sup> , G. Bagliesi<sup>a</sup> , V. Bertacchi<sup>a,c</sup> , L. Bianchini<sup>a</sup> , T. Boccali<sup>a</sup> , E. Bossini<sup>a,b</sup> , R. Castaldi<sup>a</sup> , M.A. Ciocci<sup>a,b</sup> , V. D'Amante<sup>a,d</sup> , R. Dell'Orso<sup>a</sup> , M.R. Di Domenico<sup>a,d</sup> , S. Donato<sup>a</sup> , A. Giassi<sup>a</sup> , F. Ligabue<sup>a,c</sup> , E. Manca<sup>a,c</sup> , G. Mandorli<sup>a,c</sup> , A. Messineo<sup>a,b</sup> , F. Palla<sup>a</sup> , S. Parolia<sup>a,b</sup>, G. Ramirez-Sanchez<sup>a,c</sup>, A. Rizzi<sup>a,b</sup> , G. Rolandi<sup>a,c</sup> , S. Roy Chowdhury<sup>a,c</sup>, A. Scribano<sup>a</sup>, N. Shafiei<sup>a,b</sup> , P. Spagnolo<sup>a</sup> , R. Tenchini<sup>a</sup> , G. Tonelli<sup>a,b</sup> , N. Turini<sup>a,d</sup> , A. Venturi<sup>a</sup> , P.G. Verdini<sup>a</sup> 

**INFN Sezione di Roma <sup>a</sup>, Rome, Italy, Sapienza Università di Roma <sup>b</sup>, Rome, Italy**

P. Barria<sup>a</sup> , M. Campana<sup>a,b</sup>, F. Cavallari<sup>a</sup> , D. Del Re<sup>a,b</sup> , E. Di Marco<sup>a</sup> , M. Diemoz<sup>a</sup> , E. Longo<sup>a,b</sup> , P. Meridiani<sup>a</sup> , G. Organtini<sup>a,b</sup> , F. Pandolfi<sup>a</sup>, R. Paramatti<sup>a,b</sup> , C. Quaranta<sup>a,b</sup>, S. Rahatlou<sup>a,b</sup> , C. Rovelli<sup>a</sup> , F. Santanastasio<sup>a,b</sup> , L. Soffi<sup>a</sup> , R. Tramontano<sup>a,b</sup>

**INFN Sezione di Torino <sup>a</sup>, Torino, Italy, Università di Torino <sup>b</sup>, Torino, Italy, Università del Piemonte Orientale <sup>c</sup>, Novara, Italy**

N. Amapane<sup>a,b</sup> , R. Arcidiacono<sup>a,c</sup> , S. Argiro<sup>a,b</sup> , M. Arneodo<sup>a,c</sup> , N. Bartosik<sup>a</sup> , R. Bellan<sup>a,b</sup> , A. Bellora<sup>a,b</sup> , J. Berenguer Antequera<sup>a,b</sup> , C. Biino<sup>a</sup> , N. Cartiglia<sup>a</sup> , S. Cometti<sup>a</sup> , M. Costa<sup>a,b</sup> , R. Covarelli<sup>a,b</sup> , N. Demaria<sup>a</sup> , B. Kiani<sup>a,b</sup> , F. Legger<sup>a</sup> , C. Mariotti<sup>a</sup> , S. Maselli<sup>a</sup> , E. Migliore<sup>a,b</sup> , E. Monteil<sup>a,b</sup> , M. Monteno<sup>a</sup> , M.M. Obertino<sup>a,b</sup> , G. Ortona<sup>a</sup> , L. Pacher<sup>a,b</sup> , N. Pastrone<sup>a</sup> , M. Pelliccioni<sup>a</sup> , G.L. Pinna Angioni<sup>a,b</sup>, M. Ruspa<sup>a,c</sup> , K. Shchelina<sup>a</sup> , F. Siviero<sup>a,b</sup> , V. Sola<sup>a</sup> , A. Solano<sup>a,b</sup> , D. Soldi<sup>a,b</sup> , A. Staiano<sup>a</sup> , M. Tornago<sup>a,b</sup>, D. Trocino<sup>a</sup> , A. Vagnerini<sup>a,b</sup>

**INFN Sezione di Trieste <sup>a</sup>, Trieste, Italy, Università di Trieste <sup>b</sup>, Trieste, Italy**

S. Belforte<sup>a</sup> , V. Candelise<sup>a,b</sup> , M. Casarsa<sup>a</sup> , F. Cossutti<sup>a</sup> , A. Da Rold<sup>a,b</sup> , G. Della Ricca<sup>a,b</sup> , G. Sorrentino<sup>a,b</sup>, F. Vazzoler<sup>a,b</sup> 

**Kyungpook National University, Daegu, Korea**

S. Dogra , C. Huh , B. Kim, D.H. Kim , G.N. Kim , J. Kim, J. Lee, S.W. Lee , C.S. Moon , Y.D. Oh , S.I. Pak, B.C. Radburn-Smith, S. Sekmen , Y.C. Yang

**Chonnam National University, Institute for Universe and Elementary Particles, Kwangju, Korea**

H. Kim , D.H. Moon 

**Hanyang University, Seoul, Korea**

B. Francois , T.J. Kim , J. Park 

**Korea University, Seoul, Korea**

S. Cho, S. Choi , Y. Go, B. Hong , K. Lee, K.S. Lee , J. Lim, J. Park, S.K. Park, J. Yoo

**Kyung Hee University, Department of Physics, Seoul, Republic of Korea, Seoul, Korea**

J. Goh , A. Gurtu

**Sejong University, Seoul, Korea**

H.S. Kim , Y. Kim

**Seoul National University, Seoul, Korea**

J. Almond, J.H. Bhyun, J. Choi, S. Jeon, J. Kim, J.S. Kim, S. Ko, H. Kwon, H. Lee , S. Lee, B.H. Oh, M. Oh , S.B. Oh, H. Seo , U.K. Yang, I. Yoon 

**University of Seoul, Seoul, Korea**

W. Jang, D.Y. Kang, Y. Kang, S. Kim, B. Ko, J.S.H. Lee , Y. Lee, I.C. Park, Y. Roh, M.S. Ryu, D. Song, I.J. Watson , S. Yang

**Yonsei University, Department of Physics, Seoul, Korea**

S. Ha, H.D. Yoo

**Sungkyunkwan University, Suwon, Korea**

M. Choi, H. Lee, Y. Lee, I. Yu 

**College of Engineering and Technology, American University of the Middle East (AUM), Egaila, Kuwait, Dasman, Kuwait**

T. Beyrouthy, Y. Maghrbi

**Riga Technical University, Riga, Latvia**

T. Torims, V. Veckalns<sup>47</sup> 

**Vilnius University, Vilnius, Lithuania**

M. Ambrozas, A. Carvalho Antunes De Oliveira , A. Juodagalvis , A. Rinkevicius , G. Tamulaitis 

**National Centre for Particle Physics, Universiti Malaya, Kuala Lumpur, Malaysia**

N. Bin Norjoharuddeen , W.A.T. Wan Abdullah, M.N. Yusli, Z. Zolkapli

**Universidad de Sonora (UNISON), Hermosillo, Mexico**

J.F. Benitez , A. Castaneda Hernandez , M. León Coello, J.A. Murillo Quijada , A. Sehrawat, L. Valencia Palomo 

**Centro de Investigacion y de Estudios Avanzados del IPN, Mexico City, Mexico**

G. Ayala, H. Castilla-Valdez, E. De La Cruz-Burelo , I. Heredia-De La Cruz<sup>48</sup> , R. Lopez-Fernandez, C.A. Mondragon Herrera, D.A. Perez Navarro, A. Sánchez Hernández 

**Universidad Iberoamericana, Mexico City, Mexico**

S. Carrillo Moreno, C. Oropeza Barrera , F. Vazquez Valencia

**Benemerita Universidad Autonoma de Puebla, Puebla, Mexico**

I. Pedraza, H.A. Salazar Ibarguen, C. Uribe Estrada

**University of Montenegro, Podgorica, Montenegro**

J. Mijuskovic<sup>49</sup>, N. Raicevic

**University of Auckland, Auckland, New Zealand**

D. Kofcheck 

**University of Canterbury, Christchurch, New Zealand**

P.H. Butler 

**National Centre for Physics, Quaid-I-Azam University, Islamabad, Pakistan**

A. Ahmad, M.I. Asghar, A. Awais, M.I.M. Awan, H.R. Hoorani, W.A. Khan, M.A. Shah, M. Shoaib , M. Waqas 

**AGH University of Science and Technology Faculty of Computer Science, Electronics and Telecommunications, Krakow, Poland**

V. Avati, L. Grzanka, M. Malawski

**National Centre for Nuclear Research, Swierk, Poland**

H. Bialkowska, M. Bluj , B. Boimska , M. Górska, M. Kazana, M. Szleper , P. Zalewski

**Institute of Experimental Physics, Faculty of Physics, University of Warsaw, Warsaw, Poland**

K. Bunkowski, K. Doroba, A. Kalinowski , M. Konecki , J. Krolikowski , M. Walczak 

**Laboratório de Instrumentação e Física Experimental de Partículas, Lisboa, Portugal**

M. Araujo, P. Bargassa , D. Bastos, A. Boletti , P. Faccioli , M. Gallinaro , J. Hollar , N. Leonardo , T. Niknejad, M. Pisano, J. Seixas , O. Toldaiev , J. Varela 

**Joint Institute for Nuclear Research, Dubna, Russia**

S. Afanasiev, D. Budkouski, I. Golutvin, I. Gorbunov , V. Karjavine, V. Korenkov , A. Lanev, A. Malakhov, V. Matveev<sup>50,51</sup>, V. Palichik, V. Perelygin, M. Savina, D. Seitova, V. Shalaev, S. Shmatov, S. Shulha, V. Smirnov, O. Teryaev, N. Voitishin, B.S. Yuldashev<sup>52</sup>, A. Zarubin, I. Zhizhin

**Petersburg Nuclear Physics Institute, Gatchina (St. Petersburg), Russia**

G. Gavrilov , V. Golovtcov, Y. Ivanov, V. Kim<sup>53</sup> , E. Kuznetsova<sup>54</sup> , V. Murzin, V. Oreshkin, I. Smirnov, D. Sosnov , V. Sulimov, L. Uvarov, S. Volkov, A. Vorobyev

**Institute for Nuclear Research, Moscow, Russia**

Yu. Andreev , A. Dermenev, S. Glinenko , N. Golubev, A. Karneyeu , D. Kirpichnikov , M. Kirsanov, N. Krasnikov, A. Pashenkov, G. Pivovarov , A. Toropin

**Institute for Theoretical and Experimental Physics named by A.I. Alikhanov of NRC 'Kurchatov Institute', Moscow, Russia**

V. Epshteyn, V. Gavrilov, N. Lychkovskaya, A. Nikitenko<sup>55</sup>, V. Popov, A. Stepennov, M. Toms, E. Vlasov , A. Zhokin

**Moscow Institute of Physics and Technology, Moscow, Russia**

T. Aushev

**National Research Nuclear University 'Moscow Engineering Physics Institute' (MEPhI), Moscow, Russia**

M. Chadeeva<sup>56</sup> , A. Oskin, P. Parygin, E. Popova, D. Selivanova, E. Zhemchugov<sup>56</sup> 

**P.N. Lebedev Physical Institute, Moscow, Russia**

V. Andreev, M. Azarkin, I. Dremin , M. Kirakosyan, A. Terkulov

**Skobeltsyn Institute of Nuclear Physics, Lomonosov Moscow State University, Moscow, Russia**

A. Belyaev, E. Boos , V. Bunichev, M. Dubinin<sup>57</sup> , L. Dudko , A. Gribushin, A. Kaminskiy<sup>58</sup>, V. Klyukhin , O. Kodolova , I. Lokhtin , S. Obraztsov, M. Perfilov,

V. Savrin

**Novosibirsk State University (NSU), Novosibirsk, Russia**

V. Blinov<sup>59</sup>, T. Dimova<sup>59</sup>, L. Kardapoltsev<sup>59</sup>, A. Kozyrev<sup>59</sup>, I. Ovtin<sup>59</sup>, Y. Skovpen<sup>59</sup> 

**Institute for High Energy Physics of National Research Centre 'Kurchatov Institute', Protvino, Russia**

I. Azhgirey , I. Bayshev, D. Elumakhov, V. Kachanov, D. Konstantinov , P. Mandrik , V. Petrov, R. Ryutin, S. Slabospitskii , A. Sobol, S. Troshin , N. Tyurin, A. Uzunian, A. Volkov

**National Research Tomsk Polytechnic University, Tomsk, Russia**

A. Babaev, V. Okhotnikov

**Tomsk State University, Tomsk, Russia**

V. Borshch, V. Ivanchenko , E. Tcherniaev 

**University of Belgrade: Faculty of Physics and VINCA Institute of Nuclear Sciences, Belgrade, Serbia**

P. Adzic<sup>60</sup> , M. Dordevic , P. Milenovic , J. Milosevic 

**Centro de Investigaciones Energéticas Medioambientales y Tecnológicas (CIEMAT), Madrid, Spain**

M. Aguilar-Benitez, J. Alcaraz Maestre , A. Álvarez Fernández, I. Bachiller, M. Barrio Luna, Cristina F. Bedoya , C.A. Carrillo Montoya , M. Cepeda , M. Cerrada, N. Colino , B. De La Cruz, A. Delgado Peris , J.P. Fernández Ramos , J. Flix , M.C. Fouz , O. Gonzalez Lopez , S. Goy Lopez , J.M. Hernandez , M.I. Josa , J. León Holgado , D. Moran, Á. Navarro Tobar , C. Perez Dengra, A. Pérez-Calero Yzquierdo , J. Puerta Pelayo , I. Redondo , L. Romero, S. Sánchez Navas, L. Urda Gómez , C. Willmott

**Universidad Autónoma de Madrid, Madrid, Spain**

J.F. de Trocóniz, R. Reyes-Almanza 

**Universidad de Oviedo, Instituto Universitario de Ciencias y Tecnologías Espaciales de Asturias (ICTEA), Oviedo, Spain**

B. Alvarez Gonzalez , J. Cuevas , C. Erice , J. Fernandez Menendez , S. Folgueras , I. Gonzalez Caballero , J.R. González Fernández, E. Palencia Cortezon , C. Ramón Álvarez, V. Rodríguez Bouza , A. Soto Rodríguez, A. Trapote, N. Trevisani , C. Vico Villalba

**Instituto de Física de Cantabria (IFCA), CSIC-Universidad de Cantabria, Santander, Spain**

J.A. Brochero Cifuentes , I.J. Cabrillo, A. Calderon , J. Duarte Campderros , M. Fernández , C. Fernandez Madrazo , P.J. Fernández Manteca , A. García Alonso, G. Gomez, C. Martinez Rivero, P. Martinez Ruiz del Arbol , F. Matorras , P. Matorras Cuevas , J. Piedra Gomez , C. Prieels, T. Rodrigo , A. Ruiz-Jimeno , L. Scodellaro , I. Vila, J.M. Vizan Garcia 

**University of Colombo, Colombo, Sri Lanka**

M.K. Jayananda, B. Kailasapathy<sup>61</sup>, D.U.J. Sonnadara, D.D.C. Wickramarathna

**University of Ruhuna, Department of Physics, Matara, Sri Lanka**

W.G.D. Dharmaratna , K. Liyanage, N. Perera, N. Wickramage

**CERN, European Organization for Nuclear Research, Geneva, Switzerland**

T.K. Arrestad , D. Abbaneo, J. Alimena , E. Auffray, G. Auzinger, J. Baechler, P. Baillon<sup>†</sup>, D. Barney , J. Bendavid, M. Bianco , A. Bocci , T. Camporesi, M. Capeans Garrido , G. Cerminara, N. Chernyavskaya , S.S. Chhibra , M. Cipriani , L. Cristella 

D. d'Enterria , A. Dabrowski , A. David , A. De Roeck , M.M. Defranchis , M. Deile , M. Dobson, M. Dünser , N. Dupont, A. Elliott-Peisert, N. Emriskova, F. Fallavollita<sup>62</sup>, D. Fasanella , A. Florent , G. Franzoni , W. Funk, S. Giani, D. Gigi, K. Gill, F. Glege, L. Gouskos , M. Haranko , J. Hegeman , V. Innocente , T. James, P. Janot , J. Kaspar , J. Kieseler , M. Komm , N. Kratochwil, C. Lange , S. Laurila, P. Lecoq , A. Lintuluoto, K. Long , C. Lourenço , B. Maier, L. Malgeri , S. Mallios, M. Mannelli, A.C. Marini , F. Meijers, S. Mersi , E. Meschi , F. Moortgat , M. Mulders , S. Orfanelli, L. Orsini, F. Pantaleo , L. Pape, E. Perez, M. Peruzzi , A. Petrilli, G. Petrucciani , A. Pfeiffer , M. Pierini , D. Piparo, M. Pitt , H. Qu , T. Quast, D. Rabady , A. Racz, G. Reales Gutierrez, M. Rieger , M. Rovere, H. Sakulin, J. Salfeld-Nebgen , S. Scarfi, C. Schäfer, C. Schwick, M. Selvaggi , A. Sharma, P. Silva , W. Snoeys , P. Sphicas<sup>63</sup> , S. Summers , K. Tatar , V.R. Tavolaro , D. Treille, P. Tropea, A. Tsirou, G.P. Van Onsem , J. Wanczyk<sup>64</sup>, K.A. Wozniak, W.D. Zeuner

#### **Paul Scherrer Institut, Villigen, Switzerland**

L. Caminada<sup>65</sup> , A. Ebrahimi , W. Erdmann, R. Horisberger, Q. Ingram, H.C. Kaestli, D. Kotlinski, U. Langenegger, M. Missiroli<sup>65</sup> , L. Noehte<sup>65</sup>, T. Rohe

#### **ETH Zurich - Institute for Particle Physics and Astrophysics (IPA), Zurich, Switzerland**

K. Androsov<sup>64</sup> , M. Backhaus , P. Berger, A. Calandri , A. De Cosa, G. Dissertori , M. Dittmar, M. Donegà, C. Dorfer , F. Eble, K. Gedia, F. Glessgen, T.A. Gómez Espinosa , C. Grab , D. Hits, W. Lustermann, A.-M. Lyon, R.A. Manzoni , L. Marchese , C. Martin Perez, M.T. Meinhard, F. Nessi-Tedaldi, J. Niedziela , F. Pauss, V. Perovic, S. Pigazzini , M.G. Ratti , M. Reichmann, C. Reissel, T. Reitenspiess, B. Ristic , D. Ruini, D.A. Sanz Becerra , V. Stampf, J. Steggemann<sup>64</sup> , R. Wallny , D.H. Zhu

#### **Universität Zürich, Zurich, Switzerland**

C. Amsler<sup>66</sup> , P. Bärtschi, C. Botta , D. Brzhechko, M.F. Canelli , K. Cormier, A. De Wit , R. Del Burgo, J.K. Heikkilä , M. Huwiler, W. Jin, A. Jofrehei , B. Kilminster , S. Leontsinis , S.P. Liechti, A. Macchiolo , P. Meiring, V.M. Mikuni , U. Molinatti, I. Neutelings, A. Reimers, P. Robmann, S. Sanchez Cruz , K. Schweiger , Y. Takahashi 

#### **National Central University, Chung-Li, Taiwan**

C. Adloff<sup>67</sup>, C.M. Kuo, W. Lin, A. Roy , T. Sarkar<sup>37</sup> , S.S. Yu

#### **National Taiwan University (NTU), Taipei, Taiwan**

L. Ceard, Y. Chao, K.F. Chen , P.H. Chen , W.-S. Hou , Y.y. Li, R.-S. Lu, E. Paganis , A. Psallidas, A. Steen, H.y. Wu, E. Yazgan , P.r. Yu

#### **Chulalongkorn University, Faculty of Science, Department of Physics, Bangkok, Thailand**

B. Asavapibhop , C. Asawatangtrakuldee , N. Srimanobhas 

#### **Çukurova University, Physics Department, Science and Art Faculty, Adana, Turkey**

F. Boran , S. Damarseckin<sup>68</sup>, Z.S. Demiroglu , F. Dolek , I. Dumanoglu<sup>69</sup> , E. Eskut, Y. Guler<sup>70</sup> , E. Gurpinar Guler<sup>70</sup> , I. Hos<sup>71</sup>, C. Isik, O. Kara, A. Kayis Topaksu, U. Kiminsu , G. Onengut, K. Ozdemir<sup>72</sup>, A. Polatoz, A.E. Simsek , B. Tali<sup>73</sup>, U.G. Tok , S. Turkcapar, I.S. Zorbakir , C. Zorbilmez

#### **Middle East Technical University, Physics Department, Ankara, Turkey**

B. Isildak<sup>74</sup>, G. Karapinar<sup>75</sup>, K. Ocalan<sup>76</sup> , M. Yalvac<sup>77</sup> 

#### **Bogazici University, Istanbul, Turkey**

B. Akgun, I.O. Atakisi , E. Gülmез , M. Kaya<sup>78</sup> , O. Kaya<sup>79</sup>, Ö. Özçelik, S. Tekten<sup>80</sup>, E.A. Yetkin<sup>81</sup> 

**Istanbul Technical University, Istanbul, Turkey**A. Cakir , K. Cankocak<sup>69</sup> , Y. Komurcu, S. Sen<sup>82</sup> **Istanbul University, Istanbul, Turkey**S. Cerci<sup>73</sup>, B. Kaynak, S. Ozkorucuklu, D. Sunar Cerci<sup>73</sup> **Institute for Scintillation Materials of National Academy of Science of Ukraine, Kharkov, Ukraine**

B. Grynyov

**National Scientific Center, Kharkov Institute of Physics and Technology, Kharkov, Ukraine**L. Levchuk **University of Bristol, Bristol, United Kingdom**D. Anthony, E. Bhal , S. Bologna, J.J. Brooke , A. Bundock , E. Clement , D. Cussans , H. Flacher , J. Goldstein , G.P. Heath, H.F. Heath , L. Kreczko , B. Krikler , S. Paramesvaran, S. Seif El Nasr-Storey, V.J. Smith, N. Stylianou<sup>83</sup> , K. Walkingshaw Pass, R. White**Rutherford Appleton Laboratory, Didcot, United Kingdom**K.W. Bell, A. Belyaev<sup>84</sup> , C. Brew , R.M. Brown, D.J.A. Cockerill, C. Cooke, K.V. Ellis, K. Harder, S. Harper, M.-L. Holmberg<sup>85</sup>, J. Linacre , K. Manolopoulos, D.M. Newbold , E. Olaiya, D. Petyt, T. Reis , T. Schuh, C.H. Shepherd-Themistocleous, I.R. Tomalin, T. Williams **Imperial College, London, United Kingdom**R. Bainbridge , P. Bloch , S. Bonomally, J. Borg , S. Breeze, O. Buchmuller, V. Cepaitis , G.S. Chahal<sup>86</sup> , D. Colling, P. Dauncey , G. Davies , M. Della Negra , S. Fayer, G. Fedi , G. Hall , M.H. Hassanshahi, G. Iles, J. Langford, L. Lyons, A.-M. Magnan, S. Malik, A. Martelli , D.G. Monk, J. Nash<sup>87</sup> , M. Pesaresi, D.M. Raymond, A. Richards, A. Rose, E. Scott , C. Seez, A. Shtipliyski, A. Tapper , K. Uchida, T. Virdee<sup>20</sup> , M. Vojinovic , N. Wardle , S.N. Webb , D. Winterbottom**Brunel University, Uxbridge, United Kingdom**K. Coldham, J.E. Cole , A. Khan, P. Kyberd , I.D. Reid , L. Teodorescu, S. Zahid **Baylor University, Waco, Texas, USA**S. Abdullin , A. Brinkerhoff , B. Caraway , J. Dittmann , K. Hatakeyama , A.R. Kanuganti, B. McMaster , N. Pastika, M. Saunders , S. Sawant, C. Sutantawibul, J. Wilson **Catholic University of America, Washington, DC, USA**R. Bartek , A. Dominguez , R. Uniyal , A.M. Vargas Hernandez**The University of Alabama, Tuscaloosa, Alabama, USA**A. Buccilli , S.I. Cooper , D. Di Croce , S.V. Gleyzer , C. Henderson , C.U. Perez , P. Rumerio<sup>88</sup> , C. West **Boston University, Boston, Massachusetts, USA**A. Akpinar , A. Albert , D. Arcaro , C. Cosby , Z. Demiragli , E. Fontanesi, D. Gastler, S. May , J. Rohlf , K. Salyer , D. Sperka, D. Spitzbart , I. Suarez , A. Tsatsos, S. Yuan, D. Zou**Brown University, Providence, Rhode Island, USA**G. Benelli , B. Burkle , X. Coubez<sup>21</sup>, D. Cutts , M. Hadley , U. Heintz , J.M. Hogan<sup>89</sup> 

T. KWON, G. Landsberg , K.T. Lau , D. Li, M. Lukasik, J. Luo , M. Narain, N. Pervan, S. Sagir<sup>90</sup> , F. Simpson, E. Usai , W.Y. Wong, X. Yan , D. Yu , W. Zhang

#### **University of California, Davis, Davis, California, USA**

J. Bonilla , C. Brainerd , R. Breedon, M. Calderon De La Barca Sanchez, M. Chertok , J. Conway , P.T. Cox, R. Erbacher, G. Haza, F. Jensen , O. Kukral, R. Lander, M. Mulhearn , D. Pellett, B. Regnery , D. Taylor , Y. Yao , F. Zhang 

#### **University of California, Los Angeles, California, USA**

M. Bachtis , R. Cousins , A. Datta , D. Hamilton, J. Hauser , M. Ignatenko, M.A. Iqbal, T. Lam, W.A. Nash, S. Regnard , D. Saltzberg , B. Stone, V. Valuev 

#### **University of California, Riverside, Riverside, California, USA**

K. Burt, Y. Chen, R. Clare , J.W. Gary , M. Gordon, G. Hanson , G. Karapostoli , O.R. Long , N. Manganelli, M. Olmedo Negrete, W. Si , S. Wimpenny, Y. Zhang

#### **University of California, San Diego, La Jolla, California, USA**

J.G. Branson, P. Chang , S. Cittolin, S. Cooperstein , N. Deelen , D. Diaz , J. Duarte , R. Gerosa , L. Giannini , D. Gilbert , J. Guiang, R. Kansal , V. Krutelyov , R. Lee, J. Letts , M. Masciovecchio , M. Pieri , B.V. Sathia Narayanan , V. Sharma , M. Tadel, A. Vartak , F. Würthwein , Y. Xiang , A. Yagil 

#### **University of California, Santa Barbara - Department of Physics, Santa Barbara, California, USA**

N. Amin, C. Campagnari , M. Citron , A. Dorsett, V. Dutta , J. Incandela , M. Kilpatrick , J. Kim , B. Marsh, H. Mei, M. Oshiro, M. Quinnan , J. Richman, U. Sarica , F. Setti, J. Sheplock, D. Stuart, S. Wang 

#### **California Institute of Technology, Pasadena, California, USA**

A. Bornheim , O. Cerri, I. Dutta , J.M. Lawhorn , N. Lu , J. Mao, H.B. Newman , T.Q. Nguyen , M. Spiropulu , J.R. Vlimant , C. Wang , S. Xie , Z. Zhang , R.Y. Zhu 

#### **Carnegie Mellon University, Pittsburgh, Pennsylvania, USA**

J. Alison , S. An , M.B. Andrews, P. Bryant , T. Ferguson , A. Harilal, C. Liu, T. Mudholkar , M. Paulini , A. Sanchez, W. Terrill

#### **University of Colorado Boulder, Boulder, Colorado, USA**

J.P. Cumalat , W.T. Ford , A. Hassani, E. MacDonald, R. Patel, A. Perloff , C. Savard, K. Stenson , K.A. Ulmer , S.R. Wagner 

#### **Cornell University, Ithaca, New York, USA**

J. Alexander , S. Bright-Thonney , Y. Cheng , D.J. Cranshaw , S. Hogan, J. Monroy , J.R. Patterson , D. Quach , J. Reichert , M. Reid , A. Ryd, W. Sun , J. Thom , P. Wittich , R. Zou 

#### **Fermi National Accelerator Laboratory, Batavia, Illinois, USA**

M. Albrow , M. Alyari , G. Apollinari, A. Apresyan , A. Apyan , S. Banerjee, L.A.T. Bauerdick , D. Berry , J. Berryhill , P.C. Bhat, K. Burkett , J.N. Butler, A. Canepa, G.B. Cerati , H.W.K. Cheung , F. Chlebana, M. Cremonesi, K.F. Di Petrillo , V.D. Elvira , Y. Feng, J. Freeman, Z. Gecse, L. Gray, D. Green, S. Grünendahl , O. Gutsche , R.M. Harris , R. Heller, T.C. Herwig , J. Hirschauer , B. Jayatilaka , S. Jindariani, M. Johnson, U. Joshi, T. Klijnsma , B. Klisma , K.H.M. Kwok, S. Lammel , D. Lincoln , R. Lipton, T. Liu, C. Madrid, K. Maeshima, C. Mantilla , D. Mason, P. McBride , P. Merkel, S. Mrenna , S. Nahm , J. Ngadiuba , V. O'Dell, V. Papadimitriou, K. Pedro 

C. Pena<sup>57</sup> , O. Prokofyev, F. Ravera , A. Reinsvold Hall , L. Ristori , E. Sexton-Kennedy , N. Smith , A. Soha , W.J. Spalding , L. Spiegel, S. Stoynev , J. Strait , L. Taylor , S. Tkaczyk, N.V. Tran , L. Uplegger , E.W. Vaandering , H.A. Weber 

#### **University of Florida, Gainesville, Florida, USA**

D. Acosta , P. Avery, D. Bourilkov , L. Cadamuro , V. Cherepanov, F. Errico , R.D. Field, D. Guerrero, B.M. Joshi , M. Kim, E. Koenig, J. Konigsberg , A. Korytov, K.H. Lo, K. Matchev , N. Menendez , G. Mitselmakher , A. Muthirakalayil Madhu, N. Rawal, D. Rosenzweig, S. Rosenzweig, J. Rotter, K. Shi , J. Sturdy , J. Wang , E. Yigitbasi , X. Zuo

#### **Florida State University, Tallahassee, Florida, USA**

T. Adams , A. Askew , R. Habibullah , V. Hagopian, K.F. Johnson, R. Khurana, T. Kolberg , G. Martinez, H. Prosper , C. Schiber, O. Viazlo , R. Yohay , J. Zhang

#### **Florida Institute of Technology, Melbourne, Florida, USA**

M.M. Baarmann , S. Butalla, T. Elkafrawy<sup>16</sup> , M. Hohlmann , R. Kumar Verma , D. Noonan , M. Rahmani, F. Yumiceva 

#### **University of Illinois at Chicago (UIC), Chicago, Illinois, USA**

M.R. Adams, H. Becerril Gonzalez , R. Cavanaugh , X. Chen , S. Dittmer, O. Evdokimov , C.E. Gerber , D.A. Hangal , D.J. Hofman , A.H. Merrit, C. Mills , G. Oh , T. Roy, S. Rudrabhatla, M.B. Tonjes , N. Varelas , J. Viinikainen , X. Wang, Z. Wu , Z. Ye 

#### **The University of Iowa, Iowa City, Iowa, USA**

M. Alhusseini , K. Dilsiz<sup>91</sup> , R.P. Gandrajula , O.K. Köseyan , J.-P. Merlo, A. Mestvirishvili<sup>92</sup>, J. Nachtman, H. Ogul<sup>93</sup> , Y. Onel , A. Penzo, C. Snyder, E. Tiras<sup>94</sup> 

#### **Johns Hopkins University, Baltimore, Maryland, USA**

O. Amram , B. Blumenfeld , L. Corcodilos , J. Davis, M. Eminizer , A.V. Gritsan , S. Kyriacou, P. Maksimovic , J. Roskes , M. Swartz, T.Á. Vámi 

#### **The University of Kansas, Lawrence, Kansas, USA**

A. Abreu, J. Anguiano, C. Baldenegro Barrera , P. Baringer , A. Bean , A. Bylinkin , Z. Flowers, T. Isidori, S. Khalil , J. King, G. Krintiras , A. Kropivnitskaya , M. Lazarovits, C. Lindsey, J. Marquez, N. Minafra , M. Murray , M. Nickel, C. Rogan , C. Royon, R. Salvatico , S. Sanders, E. Schmitz, C. Smith , J.D. Tapia Takaki , Q. Wang , Z. Warner, J. Williams , G. Wilson 

#### **Kansas State University, Manhattan, Kansas, USA**

S. Duric, A. Ivanov , K. Kaadze , D. Kim, Y. Maravin , T. Mitchell, A. Modak, K. Nam

#### **Lawrence Livermore National Laboratory, Livermore, California, USA**

F. Rebassoo, D. Wright

#### **University of Maryland, College Park, Maryland, USA**

E. Adams, A. Baden, O. Baron, A. Belloni , S.C. Eno , N.J. Hadley , S. Jabeen , R.G. Kellogg, T. Koeth, A.C. Mignerey, S. Nabili, C. Palmer , M. Seidel , A. Skuja , L. Wang, K. Wong 

#### **Massachusetts Institute of Technology, Cambridge, Massachusetts, USA**

D. Abercrombie, G. Andreassi, R. Bi, S. Brandt, W. Busza , I.A. Cali, Y. Chen , M. D'Alfonso , J. Eysermans, C. Freer , G. Gomez Ceballos, M. Goncharov, P. Harris, M. Hu, M. Klute , D. Kovalskyi , J. Krupa, Y.-J. Lee , C. Mironov , C. Paus , D. Rankin , C. Roland , G. Roland, Z. Shi , G.S.F. Stephans , J. Wang, Z. Wang , B. Wyslouch 

**University of Minnesota, Minneapolis, Minnesota, USA**

R.M. Chatterjee, A. Evans , P. Hansen, J. Hiltbrand, Sh. Jain , M. Krohn, Y. Kubota, J. Mans , M. Revering, R. Rusack , R. Saradhy, N. Schroeder , N. Strobbe , M.A. Wadud

**University of Nebraska-Lincoln, Lincoln, Nebraska, USA**

K. Bloom , M. Bryson, S. Chauhan , D.R. Claes, C. Fangmeier, L. Finco , F. Golf , C. Joo, I. Kravchenko , M. Musich, I. Reed, J.E. Siado, G.R. Snow<sup>†</sup>, W. Tabb, F. Yan, A.G. Zecchinelli

**State University of New York at Buffalo, Buffalo, New York, USA**

G. Agarwal , H. Bandyopadhyay , L. Hay , I. Iashvili , A. Kharchilava, C. McLean , D. Nguyen, J. Pekkanen , S. Rappoccio , A. Williams 

**Northeastern University, Boston, Massachusetts, USA**

G. Alverson , E. Barberis, Y. Haddad , A. Hortiangtham, J. Li , G. Madigan, B. Marzocchi , D.M. Morse , V. Nguyen, T. Orimoto , A. Parker, L. Skinnari , A. Tishelman-Charny, T. Wamorkar, B. Wang , A. Wisecarver, D. Wood 

**Northwestern University, Evanston, Illinois, USA**

S. Bhattacharya , J. Bueghly, Z. Chen , A. Gilbert , T. Gunter , K.A. Hahn, Y. Liu, N. Odell, M.H. Schmitt , M. Velasco

**University of Notre Dame, Notre Dame, Indiana, USA**

R. Band , R. Bucci, A. Das , N. Dev , R. Goldouzian , M. Hildreth, K. Hurtado Anampa , C. Jessop , K. Lannon , J. Lawrence, N. Loukas , D. Lutton, N. Marinelli, I. Mcalister, T. McCauley , C. Mcgrady, K. Mohrman, Y. Musienko<sup>50</sup>, R. Ruchti, P. Siddireddy, A. Townsend, M. Wayne, A. Wightman, M. Zarucki , L. Zygala

**The Ohio State University, Columbus, Ohio, USA**

B. Bylsma, B. Cardwell, L.S. Durkin , B. Francis , C. Hill , M. Nunez Ornelas , K. Wei, B.L. Winer, B.R. Yates 

**Princeton University, Princeton, New Jersey, USA**

F.M. Addesa , B. Bonham , P. Das , G. Dezoort, P. Elmer , A. Frankenthal , B. Greenberg , N. Haubrich, S. Higginbotham, A. Kalogeropoulos , G. Kopp, S. Kwan , D. Lange, D. Marlow , K. Mei , I. Ojalvo, J. Olsen , D. Stickland , C. Tully 

**University of Puerto Rico, Mayaguez, Puerto Rico, USA**

S. Malik , S. Norberg

**Purdue University, West Lafayette, Indiana, USA**

A.S. Bakshi, V.E. Barnes , R. Chawla , S. Das , L. Gutay, M. Jones , A.W. Jung , S. Karmarkar, D. Kondratyev , M. Liu, G. Negro, N. Neumeister , G. Paspalaki, C.C. Peng, S. Piperov , A. Purohit, J.F. Schulte , M. Stojanovic<sup>17</sup>, J. Thieman , F. Wang , R. Xiao , W. Xie 

**Purdue University Northwest, Hammond, Indiana, USA**

J. Dolen , N. Parashar

**Rice University, Houston, Texas, USA**

A. Baty , M. Decaro, S. Dildick , K.M. Ecklund , S. Freed, P. Gardner, F.J.M. Geurts , A. Kumar , W. Li, B.P. Padley , R. Redjimi, W. Shi , A.G. Stahl Leiton , S. Yang , L. Zhang, Y. Zhang 

**University of Rochester, Rochester, New York, USA**

A. Bodek , P. de Barbaro, R. Demina , J.L. Dulemba , C. Fallon, T. Ferbel , M. Galanti,

A. Garcia-Bellido , O. Hindrichs , A. Khukhunaishvili, E. Ranken, R. Taus

**Rutgers, The State University of New Jersey, Piscataway, New Jersey, USA**

B. Chiarito, J.P. Chou , A. Gandrakota , Y. Gershtein , E. Halkiadakis , A. Hart, M. Heindl , O. Karacheban<sup>24</sup> , I. Laflotte, A. Lath , R. Montalvo, K. Nash, M. Osherson, S. Salur , S. Schnetzer, S. Somalwar , R. Stone, S.A. Thayil , S. Thomas, H. Wang 

**University of Tennessee, Knoxville, Tennessee, USA**

H. Acharya, A.G. Delannoy , S. Fiorendi , S. Spanier 

**Texas A&M University, College Station, Texas, USA**

O. Bouhali<sup>95</sup> , M. Dalchenko , A. Delgado , R. Eusebi, J. Gilmore, T. Huang, T. Kamon<sup>96</sup>, H. Kim , S. Luo , S. Malhotra, R. Mueller, D. Overton, D. Rathjens , A. Safonov 

**Texas Tech University, Lubbock, Texas, USA**

N. Akchurin, J. Damgov, V. Hegde, S. Kunori, K. Lamichhane, S.W. Lee , T. Mengke, S. Muthumuni , T. Peltola , I. Volobouev, Z. Wang, A. Whitbeck

**Vanderbilt University, Nashville, Tennessee, USA**

E. Appelt , S. Greene, A. Gurrola , W. Johns, A. Melo, H. Ni, K. Padeken , F. Romeo , P. Sheldon , S. Tuo, J. Velkovska 

**University of Virginia, Charlottesville, Virginia, USA**

M.W. Arenton , B. Cox , G. Cummings , J. Hakala , R. Hirosky , M. Joyce , A. Ledovskoy , A. Li, C. Neu , C.E. Perez Lara , B. Tannenwald , S. White , E. Wolfe 

**Wayne State University, Detroit, Michigan, USA**

N. Poudyal 

**University of Wisconsin - Madison, Madison, WI, Wisconsin, USA**

K. Black , T. Bose , C. Caillol, S. Dasu , I. De Bruyn , P. Everaerts , F. Fienga , C. Galloni, H. He, M. Herndon , A. Hervé, U. Hussain, A. Lanaro, A. Loeliger, R. Loveless, J. Madhusudanan Sreekala , A. Mallampalli, A. Mohammadi, D. Pinna, A. Savin, V. Shang, V. Sharma , W.H. Smith , D. Teague, S. Trembath-Reichert, W. Vetens 

†: Deceased

1: Also at TU Wien, Wien, Austria

2: Also at Institute of Basic and Applied Sciences, Faculty of Engineering, Arab Academy for Science, Technology and Maritime Transport, Alexandria, Egypt

3: Also at Université Libre de Bruxelles, Bruxelles, Belgium

4: Also at Universidade Estadual de Campinas, Campinas, Brazil

5: Also at Federal University of Rio Grande do Sul, Porto Alegre, Brazil

6: Also at The University of the State of Amazonas, Manaus, Brazil

7: Also at University of Chinese Academy of Sciences, Beijing, China

8: Also at Department of Physics, Tsinghua University, Beijing, China

9: Also at UFMS, Nova Andradina, Brazil

10: Also at Nanjing Normal University Department of Physics, Nanjing, China

11: Now at The University of Iowa, Iowa City, Iowa, USA

12: Also at Institute for Theoretical and Experimental Physics named by A.I. Alikhanov of NRC 'Kurchatov Institute', Moscow, Russia

13: Also at Joint Institute for Nuclear Research, Dubna, Russia

14: Now at Cairo University, Cairo, Egypt

15: Also at British University in Egypt, Cairo, Egypt

16: Now at Ain Shams University, Cairo, Egypt

- 17: Also at Purdue University, West Lafayette, Indiana, USA  
18: Also at Université de Haute Alsace, Mulhouse, France  
19: Also at Erzincan Binali Yildirim University, Erzincan, Turkey  
20: Also at CERN, European Organization for Nuclear Research, Geneva, Switzerland  
21: Also at RWTH Aachen University, III. Physikalisches Institut A, Aachen, Germany  
22: Also at University of Hamburg, Hamburg, Germany  
23: Also at Isfahan University of Technology, Isfahan, Iran  
24: Also at Brandenburg University of Technology, Cottbus, Germany  
25: Also at Forschungszentrum Jülich, Juelich, Germany  
26: Also at Physics Department, Faculty of Science, Assiut University, Assiut, Egypt  
27: Also at Karoly Robert Campus, MATE Institute of Technology, Gyongyos, Hungary  
28: Also at Institute of Physics, University of Debrecen, Debrecen, Hungary  
29: Also at Institute of Nuclear Research ATOMKI, Debrecen, Hungary  
30: Also at MTA-ELTE Lendület CMS Particle and Nuclear Physics Group, Eötvös Loránd University, Budapest, Hungary  
31: Also at Wigner Research Centre for Physics, Budapest, Hungary  
32: Also at IIT Bhubaneswar, Bhubaneswar, India  
33: Also at Institute of Physics, Bhubaneswar, India  
34: Also at G.H.G. Khalsa College, Punjab, India  
35: Also at Shoolini University, Solan, India  
36: Also at University of Hyderabad, Hyderabad, India  
37: Also at University of Visva-Bharati, Santiniketan, India  
38: Also at Indian Institute of Technology (IIT), Mumbai, India  
39: Also at Deutsches Elektronen-Synchrotron, Hamburg, Germany  
40: Also at Sharif University of Technology, Tehran, Iran  
41: Also at Department of Physics, University of Science and Technology of Mazandaran, Behshahr, Iran  
42: Now at INFN Sezione di Bari, Università di Bari, Politecnico di Bari, Bari, Italy  
43: Also at Italian National Agency for New Technologies, Energy and Sustainable Economic Development, Bologna, Italy  
44: Also at Centro Siciliano di Fisica Nucleare e di Struttura Della Materia, Catania, Italy  
45: Also at Università di Napoli 'Federico II', Napoli, Italy  
46: Also at Consiglio Nazionale delle Ricerche - Istituto Officina dei Materiali, Perugia, Italy  
47: Also at Riga Technical University, Riga, Latvia  
48: Also at Consejo Nacional de Ciencia y Tecnología, Mexico City, Mexico  
49: Also at IRFU, CEA, Université Paris-Saclay, Gif-sur-Yvette, France  
50: Also at Institute for Nuclear Research, Moscow, Russia  
51: Now at National Research Nuclear University 'Moscow Engineering Physics Institute' (MEPhI), Moscow, Russia  
52: Also at Institute of Nuclear Physics of the Uzbekistan Academy of Sciences, Tashkent, Uzbekistan  
53: Also at St. Petersburg Polytechnic University, St. Petersburg, Russia  
54: Also at University of Florida, Gainesville, Florida, USA  
55: Also at Imperial College, London, United Kingdom  
56: Also at P.N. Lebedev Physical Institute, Moscow, Russia  
57: Also at California Institute of Technology, Pasadena, California, USA  
58: Also at INFN Sezione di Padova, Università di Padova, Padova, Italy, Università di Trento, Trento, Italy, Padova, Italy  
59: Also at Budker Institute of Nuclear Physics, Novosibirsk, Russia

- 60: Also at Faculty of Physics, University of Belgrade, Belgrade, Serbia  
61: Also at Trincomalee Campus, Eastern University, Sri Lanka, Nilaveli, Sri Lanka  
62: Also at INFN Sezione di Pavia, Università di Pavia, Pavia, Italy  
63: Also at National and Kapodistrian University of Athens, Athens, Greece  
64: Also at Ecole Polytechnique Fédérale Lausanne, Lausanne, Switzerland  
65: Also at Universität Zürich, Zurich, Switzerland  
66: Also at Stefan Meyer Institute for Subatomic Physics, Vienna, Austria  
67: Also at Laboratoire d'Annecy-le-Vieux de Physique des Particules, IN2P3-CNRS, Annecy-le-Vieux, France  
68: Also at Şırnak University, Şırnak, Turkey  
69: Also at Near East University, Research Center of Experimental Health Science, Nicosia, Turkey  
70: Also at Konya Technical University, Konya, Turkey  
71: Also at Istanbul University - Cerrahpasa, Faculty of Engineering, Istanbul, Turkey  
72: Also at Piri Reis University, Istanbul, Turkey  
73: Also at Adiyaman University, Adiyaman, Turkey  
74: Also at Ozyegin University, Istanbul, Turkey  
75: Also at Izmir Institute of Technology, Izmir, Turkey  
76: Also at Necmettin Erbakan University, Konya, Turkey  
77: Also at Bozok Üniversitesi Rektörlüğü, Yozgat, Turkey  
78: Also at Marmara University, Istanbul, Turkey  
79: Also at Milli Savunma University, Istanbul, Turkey  
80: Also at Kafkas University, Kars, Turkey  
81: Also at İstanbul Bilgi University, İstanbul, Turkey  
82: Also at Hacettepe University, Ankara, Turkey  
83: Also at Vrije Universiteit Brussel, Brussel, Belgium  
84: Also at School of Physics and Astronomy, University of Southampton, Southampton, United Kingdom  
85: Also at Rutherford Appleton Laboratory, Didcot, United Kingdom  
86: Also at IPPP Durham University, Durham, United Kingdom  
87: Also at Monash University, Faculty of Science, Clayton, Australia  
88: Also at Università di Torino, Torino, Italy  
89: Also at Bethel University, St. Paul, Minneapolis, USA  
90: Also at Karamanoğlu Mehmetbey University, Karaman, Turkey  
91: Also at Bingöl University, Bingöl, Turkey  
92: Also at Georgian Technical University, Tbilisi, Georgia  
93: Also at Sinop University, Sinop, Turkey  
94: Also at Erciyes University, Kayseri, Turkey  
95: Also at Texas A&M University at Qatar, Doha, Qatar  
96: Also at Kyungpook National University, Daegu, Korea